Fog Radio Access Networks: Ginibre Point Process Modeling and Analysis

Han-Bae Kong, *Member, IEEE*, Ian Flint, Ping Wang, *Senior Member, IEEE*, Dusit Niyato, *Fellow, IEEE*, and Nicolas Privault

Abstract

In this paper, we consider fog radio access networks (F-RANs) consisting of cache-enabled device-to-device (D2D) transmitters and fog access points (F-APs), which deliver data by exploiting cached contents or leveraging a cloud processing. We consider three types of modes at a typical user, namely D2D, F-AP and cooperative modes. In the D2D and the F-AP modes, when the user requests a content, the user receives the content from a D2D transmitter and an F-AP caching the content, respectively. In the cooperative mode, F-APs located near the user send data aided by a centralized cloud processing unit. We also examine a mode selection algorithm in which the user adaptively selects one of the three modes. In practical scenarios, to mitigate interference, the transmitters may not be placed close to each other, and thus there may exist a form of repulsion among the transmitters' locations. In this context, we model the spatial distributions of the D2D transmitters and the F-APs as β-Ginibre point processes, which reflect the repulsive behavior and contain the Poisson point process as a special case. Then, we provide analytical expressions for the coverage probabilities in the F-RANs. Our results are corroborated by Monte-Carlo simulations.

Index Terms

Fog computing, radio access networks, edge caching, device-to-device communications, repulsive point process, Ginibre point process, stochastic geometry.

I. Introduction

With the growth of various multimedia services, demand for high data rate communications has been explosively increasing [1]. Recently, as a promising solution to meet the demand, fog

H.-B. Kong, P. Wang and D. Niyato are with the School of Computer Science and Engineering, Nanyang Technological University, Singapore 639798 (e-mail: hbkong@ntu.edu.sg; wangping@ntu.edu.sg; dniyato@ntu.edu.sg). I. Flint and N. Privault are with the School of Physical and Mathematical Sciences, Nanyang Technological University, Singapore 639798 (e-mail: iflint@ntu.edu.sg; nprivault@ntu.edu.sg).

radio access networks (F-RANs) have attracted a lot of attention [2]. In the F-RANs, fog access points (F-APs) are connected via fronthaul links to a centralized baseband signal processing unit, and are endowed with caching capabilities to cache contents proactively. In this paper, we investigate the performance of the F-RANs by modeling the spatial distribution of F-APs in the networks as a β-Ginibre point process (GPP), which accounts for repulsion among the locations of the F-APs and includes the Poisson point process (PPP) as a particular case.

A. Related Work and Motivations

Lately, cloud radio access networks (C-RANs), which mitigate the baseband signal processing from distributed remote radio heads (RRHs) to centralized processors, have been recognized as a technique to achieve a high spectral and energy efficiencies [3]. In the C-RANs, the RRHs are linked to centralized control units via finite-capacity fronthaul links which carry information about the baseband signals. In [4], a robust distributed compression strategy for uplink C-RANs was developed. The authors in [5] proposed a precoding method for downlink C-RANs. By assuming PPP distributed RRHs, the performance of the C-RANs was characterized in [6]–[9]. The authors in [6] analyzed the downlink coverage probability of heterogeneous C-RANs and the work in [7] presented the outage performance of downlink C-RANs where RRHs are equipped with multiple antennas. Also, the ergodic capacity of uplink C-RANs with a distributed beamforming was examined in [8]. The coverage probability of a low complexity antenna selection algorithm for uplink C-RANs was analyzed in [9].

It was reported in [10] that an exponential growth of mobile data traffic is mainly driven by on-demand video streaming. Delivering large volume of data from content providers to end users incurs traffic congestion in backhaul links, which results in slow transmission rate and high latency. As a means to alleviate the congestion, caching popular contents at the edge of the networks has garnered significant interest [11]. The authors in [12] studied the content placement problem in a wireless network consisting of caching helpers and wireless users. In [13], both deterministic caching and random caching strategies for a wireless device-to-device (D2D) caching network were proposed. The performance of caching wireless networks was investigated in [14]–[17]. The work in [14] and [15] analyzed the outage probability of cache-enabled small-cell networks with/without underlying macro cellular network, respectively, when the locations of nodes in the networks are assumed to follow PPPs. Additionally, the coverage probability

of cache-enabled D2D networks was characterized by modeling the spatial distribution of the devices as a PPP in [16] and a Poisson cluster process in [17].

Recently, inspired by the advantages of C-RANs and caching networks, an evolution of the C-RAN, called *F-RAN*, which allows the RRHs to be equipped with local caches, has been considered as an emerging architecture for the next generation wireless networks [2]. In the F-RANs, the RRHs with cache storage, called *F-APs*, deliver data to users by exploiting cached contents or leveraging processing at a centralized unit. The authors in [18] developed joint cloud and edge processing methods for the maximization of the minimum delivery rate considering the fronthaul capacity. In [19], the interplay between cloud processing and edge caching in the F-RANs was introduced by examining the fundamental information-theoretic limits of the normalized delivery time. Tractable expressions for the effective capacity, which is defined as a link-level quality of service metric, were derived in [20] when the locations of nodes follow PPPs. In addition, the work in [21] investigated the coverage probability and the ergodic capacity of the F-RANs with PPP distributed F-APs and D2D users.

In practical networks, in order to alleviate interference or increase coverage area, transmitters in wireless networks may not be placed close to each other, and hence there may exist repulsion among the locations of the transmitters [22], [23]. In this context, determinantal point processes (DPPs), which can take the repulsive nature into account, have been adopted as the models for various wireless networks [24]–[29]. In [24], the signal-to-interference ratio (SIR) distribution in cellular networks modeled by Gauss, Cauchy and generalized gamma DPPs was characterized. The GPP [30] is a special case of the DPP. The α-GPP $(-1 \leq \alpha < 0)$ is a superposition of $-1/\alpha$ independent GPPs [31]. The authors in [25] and [26] provided analytical expressions for the performance of wireless sensor networks with/without a fractional channel inversion power control, respectively. Another kind of parametrization of the GPP is the so-called β-GPP $(0 < \beta \leq 1)$ which is a thinned and re-scaled GPP, generated by retaining each point of the GPP independently with probability β [32]. Exploiting the specificities of the β-GPP, the coverage probabilities in single-tier and heterogeneous cellular networks were analyzed in [27] and [28], respectively. In addition, in [29], it has been observed that the β-GPP is a realistic model for the locations of base stations.

It should be remarked that the previous works on F-RANs in [20] and [21] assumed that the locations of nodes in the F-RANs follow PPPs due to its analytical simplicity. Despite the fact that F-APs in practical F-RANs may experience a repulsive nature, the performance of the

F-RANs, which takes the repulsion into account has not been studied yet. Therefore, in this paper, we analyze the coverage probability of the F-RANs by modeling the spatial distribution of the F-APs in the F-RANs as a β-GPP.

B. Contributions and Organization

In this paper, we study F-RANs consisting of cache-enabled D2D transmitters and F-APs. Three types of user access modes are considered when a typical user requests a content, namely D2D, F-AP and cooperative modes. In the D2D mode, the user receives the content from a D2D transmitter which caches the content. An F-AP possessing the content delivers data to the user in the F-AP mode. Lastly, in the cooperative mode, multiple F-APs transmit the content aided by the centralized unit. Considering the three types of modes, we derive analytical expressions for the coverage probability, which is the probability that the received SIR is higher than a certain SIR threshold, when the locations of the D2D transmitters and the F-APs are assumed to follow independent β-GPPs. The contributions of this paper are detailed as follows.

- In the D2D (or F-AP) mode, the typical user is associated with the closest D2D transmitter (or F-AP) which caches the requested content and is within a distance. Under this setup, the interference can be decomposed into three terms. For example, in the F-AP mode, there exist interferences from the D2D transmitters and the F-APs with/without the requested content. Unlike what happens in the PPP setting, when the locations of the F-APs follow a β-GPP, the interferences from the F-APs with/without the requested content are correlated. We obtain analytical expressions for the coverage probabilities in the D2D and the F-AP modes by accounting for the correlation.
- In the cooperative mode, all F-APs within a distance from the user simultaneously transmit data using a distributed beamforming [8]. We provide an approximation of the coverage probability in this mode. In the specific case wherein the spatial distributions of the D2D transmitters and the F-APs are modeled by the PPP and the β-GPP, respectively, we derive another approximation of the coverage probability which has a lower computational complexity.
- In addition, as a method to take full advantage of the centralized processing and the edge caching in F-RANs, we consider a mode selection algorithm, which adaptively chooses one of the three modes. The coverage probability of the network with the mode selection

algorithm is investigated. From numerical simulation results, it is shown that a higher coverage probability can be achieved by adopting the mode selection.

- For the β-GPP, the parameter β presents the degree of the repulsion, and the β-GPP weakly converges to the PPP as $\beta \to 0$. Motivated by this fact, we derive analytical results in the PPP by letting $\beta \to 0$ in our general results. In this sense, our analysis can be considered as a generalization of the previous work in the networks driven by PPPs [21].

This paper is organized as follows. Section II presents the system model and reviews the background on the β-GPP. We analyze the coverage probabilities of the three user access modes and the mode selection algorithm in Section III. In Section IV, numerical simulation results are provided to validate our analysis. Finally, the conclusions are drawn in Section V.

Throughout the paper, we use the following notations. $\mathbb{P}(A)$ and $\mathbb{E}[X]$ represent the probability of an event A and the expectation of a random variable X, respectively. The bold notation is adopted to denote a point $\mathbf{x} \in \mathbb{R}^2$. The notations $\|\mathbf{x}\|$, $|x|$ and x^* stand for the Euclidean 2-norm of $\mathbf{x}$, Euclidean norm and conjugate of a complex scalar x, respectively. Lastly, $\Phi \sim PPP(\lambda)$ and $\Phi \sim GPP(\lambda, \beta)$ stand for the cases where a point process Φ follows a PPP with intensity λ and a β-GPP with intensity λ and repulsion parameter β, respectively. The list of the symbols used in this paper and their definitions is provided in Table I.

II. System Model and Preliminaries

A. Network model

In this paper, we investigate F-RANs comprising of cache-enabled D2D transmitters and F-APs, which are equipped with caching storage units and connected to a centralized unit as illustrated in Fig. 1. As explained previously, we consider three types of user access modes for a typical user requesting a content c, namely D2D, F-AP and cooperative modes. In the D2D (or F-AP) mode, the user is connected to the nearest D2D transmitter (or F-AP) which stores the content c and is within the distance r_D (or r_F). Here, r_D and r_F represent for the maximum distances in the D2D and the F-AP modes, respectively. In the cooperative mode, all F-APs within the distance r_C, simultaneously send data to the user employing a distributed beamforming aided by the centralized processing unit [8]. Also, we examine the mode selection algorithm choosing one of the three modes in Section II-D.

In order to take into account the repulsive nature in practical networks [22], [23], we model the spatial distributions of the D2D transmitters and the F-APs by independent β-GPPs Φ_D and

TABLE I

LIST OF SYMBOLS

Symbol	Definition	Symbol	Definition
r_D	Maximum distance for the D2D mode	λ_D	Spatial intensity of Φ_D
r_F	Maximum distance for the F-AP mode	λ_F	Spatial intensity of Φ_F
r_C	Maximum distance for the cooperative mode	β_D	Repulsion parameter of Φ_D
Φ_D	β-GPP which models the distribution of the D2D transmitters	β_F	Repulsion parameter of Φ_F
Φ_F	β-GPP which models the distribution of the F-APs	$\mathcal{C}$	Set of all contents
s_D	Size of cache storage at the D2D transmitters	M	The number of all contents
s_F	Size of cache storage at the F-APs	δ	Parameter for the Zipf distribution
η_{D_m}	Probability that a content $c_m \in \mathcal{C}$ is cached at a D2D transmitter	α	Path loss exponent
η_{F_m}	Probability that a content $c_m \in \mathcal{C}$ is cached at an F-AP	γ_{th}	SIR threshold
ξ_m	Probability that a typical user requests a content $c_m \in \mathcal{C}$	P_F	Transmit power at the F-APs
P_D	Transmit power at the D2D transmitters		

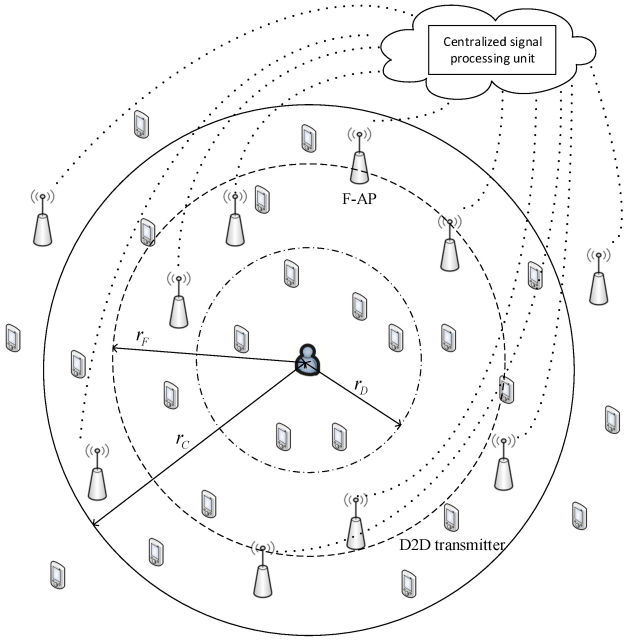

Fig. 1. The fog radio access networks.

Φ_F, respectively. The intensities of Φ_D and Φ_F are λ_D and λ_F, respectively, and β_D and β_F denote the repulsion parameters of Φ_D and Φ_F, respectively[1]. Note that the β-GPP includes the PPP as a special case. Thus, for example, we obtain the case with PPP distributed D2D

[1]When a portion of D2D transmitters (or F-APs) send signal at a given resource block, the spatial distribution of the *active* D2D transmitters (or F-APs) can be obtained by thinning Φ_D (or Φ_F).

transmitters by letting β_D go to zero.

B. Caching

Let us define a finite content category $\mathcal{C} = \{c_1, c_2, \ldots, c_M\}$ where c_m is the m-th most popular content for $m = 1, \ldots, M$. It is assumed that all contents have the same size, which is normalized to one [14], [18], [21]. We assume that each D2D transmitter and each F-AP has a cache storage of sizes s_D and s_F, respectively. Let us denote by η_{D_m} and η_{F_m} the probabilities that a content $c_m \in \mathcal{C}$ is cached at a D2D transmitter and an F-AP, respectively.

We consider two types of pre-fetching strategies respectively called *random caching strategy (RCS)* and *popularity-based caching strategy (PCS)*. For the RCS, each node randomly caches files regardless of their popularity, and thus

$$\eta_{D_m} = s_D/M \quad \text{and} \quad \eta_{F_m} = s_F/M. \tag{1}$$

For the PCS, each D2D transmitter and each F-AP proactively stores the s_D and s_F most popular files, respectively. Hence, we have

$$\eta_{D_m} = \begin{cases} 1, & \text{if } \ m \leq s_D, \\ 0, & \text{otherwise,} \end{cases} \quad \text{and} \quad \eta_{F_m} = \begin{cases} 1, & \text{if } \ m \leq s_F, \\ 0, & \text{otherwise.} \end{cases} \tag{2}$$

Since each D2D transmitter caches contents independently from other D2D transmitters, for a given content c_m, the D2D transmitters can be divided into two groups, namely the D2D transmitters which cache c_m (Φ_{D_m}) and the D2D transmitters which do not ($\tilde{\Phi}_{D_m}$) where $\Phi_{D_m} \cup \tilde{\Phi}_{D_m} = \Phi_D$. In a similar fashion, the spatial distribution of the F-APs which have c_m, and the locations of the F-APs which do not, are respectively defined as Φ_{F_m} and $\tilde{\Phi}_{F_m}$ where $\Phi_{F_m} \cup \tilde{\Phi}_{F_m} = \Phi_F$. Then, from (1) and (2), the intensities of Φ_{D_m}, $\tilde{\Phi}_{D_m}$, Φ_{F_m} and $\tilde{\Phi}_{F_m}$ are equal to $\eta_{D_m}\lambda_D$, $(1-\eta_{D_m})\lambda_D$, $\eta_{F_m}\lambda_F$ and $(1-\eta_{F_m})\lambda_F$, respectively.

It is assumed that the content popularity follows the Zipf distribution [33], and therefore the probability that the m-th most popular content c_m is requested is given by

$$\xi_m = \frac{1}{m^\delta} \left(\sum_{j=1}^{M} \frac{1}{j^\delta} \right)^{-1}. \tag{3}$$

Note that the lower indexed content has a higher popularity, i.e., $\xi_i > \xi_j$ if $i < j$. Here, $\delta (\geq 0)$ models the skewness of the popularity profile. When δ is large, only a few popular contents are frequently accessed. As a special case, when $\delta = 0$, the content popularity follows the uniform distribution, i.e., $\xi_m = 1/M$ for all m.

C. SIR

Thanks to the stationarity of the β-GPP [32], without loss of generality, we assume that the typical user is located at the origin o. First let us focus on the D2D mode. When the user requests the content c_m and the user is connected to the nearest D2D transmitter in Φ_{D_m}, we express the SIR γ_{D_m} as

$$\gamma_{D_m} = \frac{P_D h_{D_{m,o}} \|\mathbf{x}_{D_{m,o}}\|^{-\alpha}}{I_{D_m} + I_F}, \tag{4}$$

where

$$D_{m,o} = \underset{i \in \mathbb{N} \text{ s.t. } \mathbf{x}_i \in \Phi_{D_m}}{\arg\min} \|\mathbf{x}_i\|, \quad I_F = \sum_{k \in \mathbb{N} \text{ s.t. } \mathbf{x}_k \in \Phi_F} P_F g_k \|\mathbf{x}_k\|^{-\alpha}, \tag{5}$$

$$I_{D_m} = \sum_{k \in \mathbb{N} \setminus \{D_{m,o}\} \text{ s.t. } \mathbf{x}_k \in \Phi_D} P_D h_k \|\mathbf{x}_k\|^{-\alpha} = \hat{I}_{D_m} + \tilde{I}_{D_m}, \tag{6}$$

$$\hat{I}_{D_m} \triangleq \sum_{k \in \mathbb{N} \setminus \{D_{m,o}\} \text{ s.t. } \mathbf{x}_k \in \Phi_{D_m}} P_D h_k \|\mathbf{x}_k\|^{-\alpha}, \ \tilde{I}_{D_m} \triangleq \sum_{k \in \mathbb{N} \text{ s.t. } \mathbf{x}_k \in \tilde{\Phi}_{D_m}} P_D h_k \|\mathbf{x}_k\|^{-\alpha},$$

where P_D and P_F represent the transmit powers at the D2D transmitters and the F-APs, respectively. Here, α and h_k denote the path loss exponent and the gain of the small-scale fading channel between the user and the D2D transmitter located at $\mathbf{x}_k$, and g_k indicates for the gain of the small-scale fading channel between the user and the F-AP located at $\mathbf{x}_k$.

Next, for the F-AP mode, when the user accesses the content c_m and receives the content from the closest F-AP in Φ_{F_m}, the SIR γ_{F_m} is written as

$$\gamma_{F_m} = \frac{P_F g_{F_{m,o}} \|\mathbf{x}_{F_{m,o}}\|^{-\alpha}}{I_D + I_{F_m}}, \tag{7}$$

where

$$F_{m,o} = \underset{i \in \mathbb{N} \text{ s.t. } \mathbf{x}_i \in \Phi_{F_m}}{\arg\min} \|\mathbf{x}_i\|, \quad I_D = \sum_{k \in \mathbb{N} \text{ s.t. } \mathbf{x}_k \in \Phi_D} P_D h_k \|\mathbf{x}_k\|^{-\alpha}, \tag{8}$$

$$I_{F_m} = \sum_{k \in \mathbb{N} \setminus \{F_{m,o}\} \text{ s.t. } \mathbf{x}_k \in \Phi_F} P_F g_k \|\mathbf{x}_k\|^{-\alpha} = \hat{I}_{F_m} + \tilde{I}_{F_m}, \tag{9}$$

$$\hat{I}_{F_m} \triangleq \sum_{k \in \mathbb{N} \setminus \{F_{m,o}\} \text{ s.t. } \mathbf{x}_k \in \Phi_{F_m}} P_F g_k \|\mathbf{x}_k\|^{-\alpha}, \ \tilde{I}_{F_m} \triangleq \sum_{k \in \mathbb{N} \text{ s.t. } \mathbf{x}_k \in \tilde{\Phi}_{F_m}} P_F g_k \|\mathbf{x}_k\|^{-\alpha}.$$

Lastly, in the cooperative mode, the F-APs within the distance r_C deliver content to the user by leveraging the centralized unit. More specifically, the centralized unit first sends the content to those F-APs, and then coordinates the F-APs to send data simultaneously. It is assumed that the distributed beamforming transmission, which can achieve performance similar to maximal

ratio combining, is employed [8]. Then, the F-AP at $\mathbf{x}_k$ transmits a signal by multiplying the data by $\sqrt{P_F}\tilde{g}_k^*\|\mathbf{x}_k\|^{-\alpha/2}\big(\sum_{\mathbf{x}_k\in\tilde{\Phi}_F} g_k\|\mathbf{x}_k\|^{-\alpha}\big)^{-1/2}$, where $\tilde{g}_k$ stands for the small-scale fading channel between the user and the F-AP located at $\mathbf{x}_k$ ($|\tilde{g}_k|^2 = g_k$), $\tilde{\Phi}_F \triangleq \Phi_F \cap \mathcal{B}_o(r_C)$ and $\mathcal{B}_o(r)$ denotes the ball centered at the origin with radius r. Then, the SIR γ_C is given by

$$\gamma_C = \frac{\sum_{\mathbf{x}_k\in\tilde{\Phi}_F} P_F g_k\|\mathbf{x}_k\|^{-\alpha}}{\sum_{\mathbf{x}_k\in\hat{\Phi}_F} P_F g_k\|\mathbf{x}_k\|^{-\alpha} + I_D}, \tag{10}$$

where $\hat{\Phi}_F \triangleq \Phi_F \setminus \tilde{\Phi}_F$.

D. Coverage Probability

We define the coverage probability as the probability that the SIR is larger than a pre-defined SIR threshold γ_{th}. Then, the coverage probabilities for the three modes are respectively equal to

$$\mathcal{P}_{D_m} \triangleq \mathbb{P}\left(\gamma_{D_m} \geq \gamma_{th}, \|\mathbf{x}_{D_{m,o}}\| \leq r_D\right), \tag{11}$$

$$\mathcal{P}_{F_m} \triangleq \mathbb{P}\left(\gamma_{F_m} \geq \gamma_{th}, \|\mathbf{x}_{F_{m,o}}\| \leq r_F\right), \tag{12}$$

$$\mathcal{P}_C \triangleq \mathbb{P}\left(\gamma_C \geq \gamma_{th}\right). \tag{13}$$

When the typical user always operates in the D2D mode or the F-AP mode, the average coverage probabilities $\mathcal{P}_{D,cov}$ and $\mathcal{P}_{F,cov}$ are respectively given by

$$\mathcal{P}_{D,cov} = \sum_{m=1}^{M} \xi_m \mathcal{P}_{D_m}, \tag{14}$$

$$\mathcal{P}_{F,cov} = \sum_{m=1}^{M} \xi_m \mathcal{P}_{F_m}, \tag{15}$$

where ξ_m is the probability that the user requests the content c_m in (3). Note that $\mathcal{P}_C$ in (13) does not depend on the requested content, and thus the average coverage probability for the cooperative mode is equal to $\mathcal{P}_C$.

Let us consider the scenario wherein the typical user judiciously selects one of the D2D, the F-AP and the cooperative modes. To be specific, when the user accesses the content c_m, if the nearest D2D transmitter in Φ_{D_m} is within the distance r_D (i.e., $\|\mathbf{x}_{D_{m,o}}\| \leq r_D$), the user receives the content from the D2D transmitter. If $\|\mathbf{x}_{D_{m,o}}\| > r_D$, the user is associated with the closest F-AP in Φ_{F_m} when $\|\mathbf{x}_{F_{m,o}}\| \leq r_F$. When $\|\mathbf{x}_{D_{m,o}}\| > r_D$ and $\|\mathbf{x}_{F_{m,o}}\| > r_F$, all F-APs within r_C transmit data to the user after receiving the requested content from the centralized unit. Then, we write the average coverage probability for the mode selection algorithm as

$$\mathcal{P}_{cov} = \sum_{m=1}^{M} \xi_m \mathcal{P}_m, \tag{16}$$

where

$$\mathcal{P}_m \triangleq \mathcal{P}_{D_m} + \tilde{\mathcal{P}}_{F_m} + \tilde{\mathcal{P}}_{C_m}, \tag{17}$$

$$\tilde{\mathcal{P}}_{F_m} \triangleq \mathbb{P}\left(\gamma_{F_m} \geq \gamma_{th}, \|\mathbf{x}_{F_{m,o}}\| \leq r_F, \|\mathbf{x}_{D_{m,o}}\| > r_D\right), \tag{18}$$

$$\tilde{\mathcal{P}}_{C_m} \triangleq \mathbb{P}\left(\gamma_C \geq \gamma_{th}, \|\mathbf{x}_{F_{m,o}}\| > r_F, \|\mathbf{x}_{D_{m,o}}\| > r_D\right). \tag{19}$$

One may consider the scenario where the user first attempts to receive the content from an F-AP and then from a D2D transmitter. Our analysis in Section III can also be applied to this scenario.

E. Preliminaries

Let us consider the β-GPP $\Phi = \{\mathbf{x}_k\}_{k\in\mathbb{N}}$ with intensity λ and repulsion parameter β. Then, the set $\{\|\mathbf{x}_k\|^2\}_{k\in\mathbb{N}}$ has the same distribution as the set χ constructed from an i.i.d. sequence $\{B_i\}_{i\in\mathbb{N}}$ by deleting each B_i independently and with probability $1-\beta$ where $B_i \sim \mathcal{G}\left(i, \beta/\pi\lambda\right)$ and $\mathcal{G}(a,b)$ denotes a gamma random variable with shape parameter a and scale parameter b [32].

In this model, the received signal at the user from the D2D transmitter at $\mathbf{x}_k$ becomes $P_D h_k \|\mathbf{x}_k\|^{-\alpha} = P_D h_k B_{D,k}^{-\alpha/2}$ where $B_{D,k} \sim \mathcal{G}\left(k, \beta_D/\pi\lambda_D\right)$. In addition, the sum of the received signals at the user from the D2D transmitters is expressed as $\sum_{\mathbf{x}_k\in\Phi_D} P_D h_k \|\mathbf{x}_k\|^{-\alpha} = \sum_{k=1}^{\infty} P_D h_k B_{D,k}^{-\alpha/2}\Xi_{D,k}$ where $\{\Xi_{D,k}\}$ indicates a set of independent discrete random variables with $\mathbb{E}\left[\Xi_{D,k}\right] = \beta_D$ and $\Xi_{D,k} \in \{0,1\}$. Similarly, we represent the sum of the received signals at the user from the F-APs as $\sum_{\mathbf{x}_k\in\Phi_F} P_F g_k \|\mathbf{x}_k\|^{-\alpha} = \sum_{k=1}^{\infty} P_F g_k B_{F,k}^{-\alpha/2}\Xi_{F,k}$ where $B_{F,k} \sim \mathcal{G}\left(k, \beta_F/\pi\lambda_F\right)$ and $\{\Xi_{F,k}\}$ is a set of independent random variables with mean β_F and $\Xi_{F,k} \in \{0,1\}$. Here, the probability density functions (PDFs) of $B_{D,k}$ and $B_{F,k}$ are respectively given by

$$f_{B_{D,k}}(x) = \frac{x^{k-1}}{\left(\frac{\beta_D}{\pi\lambda_D}\right)^k \Gamma\left(k\right)} \exp\left(-\frac{\pi\lambda_D}{\beta_D}x\right), \; f_{B_{F,k}}(x) = \frac{x^{k-1}}{\left(\frac{\beta_F}{\pi\lambda_F}\right)^k \Gamma\left(k\right)} \exp\left(-\frac{\pi\lambda_F}{\beta_F}x\right). \tag{20}$$

Before analyzing the coverage probability, let us derive the Laplace transforms which is utilized in Section III. We denote the Laplace transform of a random variable X as $\mathcal{L}_X(s) \triangleq \mathbb{E}\left[\exp\left(-sX\right)\right]$. Then, the Laplace transforms of I_F and I_D in (5) and (8) are respectively derived as

$$\begin{aligned}\mathcal{L}_{I_F}(s) &= \mathbb{E}\left[\exp\left(-s\sum_{k=1}^{\infty} P_F g_k B_{F,k}^{-\alpha/2}\Xi_{F,k}\right)\right] = \mathbb{E}\left[\prod_{k=1}^{\infty}\exp\left(-sP_F g_k B_{F,k}^{-\alpha/2}\Xi_{F,k}\right)\right] \\ &= \mathbb{E}\left[\prod_{k=1}^{\infty}\frac{1}{1+sP_F B_{F,k}^{-\alpha/2}\Xi_{F,k}}\right] = \mathbb{E}\left[\prod_{k=1}^{\infty}\left(\frac{\beta_F}{1+sP_F B_{F,k}^{-\alpha/2}} + 1 - \beta_F\right)\right]\end{aligned}$$

$$= \prod_{k=1}^{\infty} \left(\int_0^{\infty} \frac{\beta_F}{1 + sP_F x^{-\alpha/2}} f_{B_{F,k}}(x)\, \mathrm{d}x + 1 - \beta_F \right), \tag{21}$$

$$\mathcal{L}_{I_D}(s) = \prod_{k=1}^{\infty} \left(\int_0^{\infty} \frac{\beta_D}{1 + sP_D x^{-\alpha/2}} f_{B_{D,k}}(x)\, \mathrm{d}x + 1 - \beta_D \right). \tag{22}$$

Now, we introduce the distributions of the contact distances $\|\mathbf{x}_{D_{m,o}}\|$ and $\|\mathbf{x}_{F_{m,o}}\|$. The cumulative distribution functions (CDFs) of $\|\mathbf{x}_{D_{m,o}}\|$ and $\|\mathbf{x}_{F_{m,o}}\|$ are identified as

$$F_{\|\mathbf{x}_{D_{m,o}}\|}(x) = \mathbb{P}\left(\|\mathbf{x}_{D_{m,o}}\| \leq x\right) = 1 - \mathbb{P}\left(\forall \mathbf{x}_i \in \Phi_{D_m}, \|\mathbf{x}_i\| > x\right)$$

$$= 1 - \prod_{k=1}^{\infty} \left(\eta_{D_m}\beta_D \mathbb{P}\left(B_{D,k} > x^2\right) + 1 - \eta_{D_m}\beta_D\right) = 1 - \prod_{k=1}^{\infty} \left(1 - \frac{\eta_{D_m}\beta_D}{\Gamma(k)} \gamma\left(k, \frac{\pi\lambda_D}{\beta_D} x^2\right)\right), \tag{23}$$

$$F_{\|\mathbf{x}_{F_{m,o}}\|}(x) = 1 - \prod_{k=1}^{\infty} \left(1 - \frac{\eta_{F_m}\beta_F}{\Gamma(k)} \gamma\left(k, \frac{\pi\lambda_F}{\beta_F} x^2\right)\right), \tag{24}$$

where $\gamma(a, b) = \int_0^b t^{a-1} e^{-t}\, \mathrm{d}t$ is the lower-incomplete gamma function.

When $\Phi_D \sim PPP(\lambda_D)$ and $\Phi_F \sim PPP(\lambda_F)$, the CDFs of $\|\mathbf{x}_{D_{m,o}}\|$ and $\|\mathbf{x}_{F_{m,o}}\|$ are respectively represented as [34]

$$F_{\|\mathbf{x}_{D_{m,o}}\|}(x) = 1 - \exp\left(-\pi\eta_{D_m}\lambda_D x^2\right), \; F_{\|\mathbf{x}_{F_{m,o}}\|}(x) = 1 - \exp\left(-\pi\eta_{F_m}\lambda_F x^2\right). \tag{25}$$

Additionally, the PDFs of $\|\mathbf{x}_{D_{m,o}}\|$ and $\|\mathbf{x}_{F_{m,o}}\|$ are respectively given by

$$f_{\|\mathbf{x}_{D_{m,o}}\|}(x) = 2\pi\eta_{D_m}\lambda_D x \exp\left(-\pi\eta_{D_m}\lambda_D x^2\right), \; f_{\|\mathbf{x}_{F_{m,o}}\|}(x) = 2\pi\eta_{F_m}\lambda_F x \exp\left(-\pi\eta_{F_m}\lambda_F x^2\right). \tag{26}$$

When $\Phi_F \sim PPP(\lambda_F)$ and $\Phi_D \sim PPP(\lambda_D)$, $\mathcal{L}_{I_F}$ in (21) and $\mathcal{L}_{I_D}$ in (22) can be simplified as [34]

$$\mathcal{L}_{I_F}(s) = \exp\left(-\frac{2\pi^2\lambda_F}{\alpha \sin\left(\frac{2\pi}{\alpha}\right)} (sP_F)^{2/\alpha}\right), \; \mathcal{L}_{I_D}(s) = \exp\left(-\frac{2\pi^2\lambda_D}{\alpha \sin\left(\frac{2\pi}{\alpha}\right)} (sP_D)^{2/\alpha}\right). \tag{27}$$

We remark here that proceeding as in the proof of Theorem 2, one can prove the convergence of the quantities in (21)-(22) to those in (27), which is due to the fact that the β-GPP tends to the PPP in law as β goes to zero, cf. [32].

In addition, when $\Phi_D \sim PPP(\lambda_D)$ and $\Phi_F \sim PPP(\lambda_F)$, the Laplace transform of I_{F_m} in (9) is computed as

$$\mathcal{L}_{I_{F_m}}(s, \|\mathbf{x}_{F_{m,o}}\|) = \mathcal{L}_{\hat{I}_{F_m}}(s, \|\mathbf{x}_{F_{m,o}}\|) \mathcal{L}_{\tilde{I}_{F_m}}(s), \tag{28}$$

$$\mathcal{L}_{\hat{I}_{F_m}}(s, \|\mathbf{x}_{F_{m,o}}\|) = \mathbb{E}\left[\exp\left(-s \sum_{\mathbf{x}_k \in \Phi_{F_m}} P_F g_k \|\mathbf{x}_k\|^{-\alpha} \mathbb{1}_{\{\|\mathbf{x}_k\| > \|\mathbf{x}_{F_{m,o}}\|\}}\right)\right]$$

$$= \exp\left(-2\pi\eta_{F_m}\lambda_F \int_{\|\mathbf{x}_{F_{m,o}}\|}^{\infty} \frac{x}{1+x^{\alpha}/(sP_F)}\,\mathrm{d}x\right),$$

$$\mathcal{L}_{\tilde{I}_{F_m}}(s) = \mathbb{E}\left[\exp\left(-s\sum_{\mathbf{x}_k\in\tilde{\Phi}_{F_m}} P_F g_k \|\mathbf{x}_k\|^{-\alpha}\right)\right] = \exp\left(-\frac{2\pi^2\left(1-\eta_{F_m}\right)\lambda_F}{\alpha\sin\left(\frac{2\pi}{\alpha}\right)}(sP_F)^{2/\alpha}\right).$$

Similarly to (28), the Laplace transform of I_{D_m} in (6) becomes

$$\mathcal{L}_{I_{D_m}}(s,\|\mathbf{x}_{D_{m,o}}\|) = \mathcal{L}_{\hat{I}_{D_m}}(s,\|\mathbf{x}_{D_{m,o}}\|)\mathcal{L}_{\tilde{I}_{D_m}}(s), \tag{29}$$

$$\mathcal{L}_{\hat{I}_{D_m}}(s,\|\mathbf{x}_{D_{m,o}}\|) = \exp\left(-2\pi\eta_{D_m}\lambda_D \int_{\|\mathbf{x}_{D_{m,o}}\|}^{\infty} \frac{x}{1+x^{\alpha}/(sP_D)}\,\mathrm{d}x\right),$$

$$\mathcal{L}_{\tilde{I}_{D_m}}(s) = \exp\left(-\frac{2\pi^2\left(1-\eta_{D_m}\right)\lambda_D}{\alpha\sin\left(\frac{2\pi}{\alpha}\right)}(sP_D)^{2/\alpha}\right).$$

III. Performance Analysis

In this section, we introduce expressions for the coverage probabilities in Section II-D. First, we examine the D2D, the F-AP and the cooperative modes. Then, the performance of mode selection algorithm will be investigated.

A. D2D mode

When the user requests the content c_m and it is associated with the nearest D2D transmitter which has the content c_m, we rewrite the SIR γ_{D_m} in (4) as

$$\gamma_{D_m} = \frac{P_D h_{D_{m,o}} B_{D,D_{m,o}}^{-\alpha/2}}{\sum_{k\in\mathbb{N}\setminus\{D_{m,o}\}} P_D h_k B_{D,k}^{-\alpha/2}\Xi_{D,k} + I_F}, \tag{30}$$

where $I_F = \sum_{k=1}^{\infty} P_F g_k B_{F,k}^{-\alpha/2}\Xi_{F,k}$. The expression for the coverage probability $\mathcal{P}_{D_m}$ in (11) is identified in the following theorem.

Theorem 1. *When the typical user requests the content c_m, the coverage probability $\mathcal{P}_{D_m}$ in* (11) *is expressed as*

$$\mathcal{P}_{D_m} = 2\pi\eta_{D_m}\lambda_D \int_0^{r_D} \mathcal{L}_{I_F}\left(\frac{\gamma_{th}z^{\alpha}}{P_D}\right)\exp\left(-\frac{\pi\lambda_D z^2}{\beta_D}\right)\Upsilon_{D_m}\left(\frac{\pi\lambda_D z^2}{\beta_D}\right)\Delta_{D_m}\left(\frac{\pi\lambda_D z^2}{\beta_D}\right) z\,\mathrm{d}z, \tag{31}$$

where $\mathcal{L}_{I_F}(s)$ is defined in (21) *and, for any $x>0$, we have defined*

$$\Upsilon_{D_m}(x) = \sum_{i=1}^{\infty} \frac{x^{i-1}}{\Gamma(i)}\left(A_{\eta_{D_m},\beta_D,i}(x,\gamma_{th}x^{\alpha/2})\right)^{-1}, \tag{32}$$

$$\Delta_{D_m}(x) = \prod_{k=1}^{\infty} A_{\eta_{D_m},\beta_D,k}(x, \gamma_{th} x^{\alpha/2}), \tag{33}$$

$$A_{n,b,k}(x,\tau) = 1 - b + \int_x^{\infty} \frac{nb\nu^{k-1}\exp(-\nu)}{\Gamma(k)\,(1+\tau\nu^{-\alpha/2})}\,\mathrm{d}\nu + \int_0^{\infty} \frac{(1-n)b\nu^{k-1}\exp(-\nu)}{\Gamma(k)\,(1+\tau\nu^{-\alpha/2})}\,\mathrm{d}\nu. \tag{34}$$

Proof. See Appendix A. □

When $\Phi_D \sim PPP(\lambda_D)$ and $\Phi_F \sim PPP(\lambda_F)$, we obtain an expression for the coverage probability $\mathcal{P}_{D_m}$ by letting $\beta_D \to 0$ and $\beta_F \to 0$, as presented in the following theorem.

Theorem 2. *When $\Phi_D \sim PPP(\lambda_D)$, the coverage probability $\mathcal{P}_{D_m}$ in* (11) *is given by*

$$\mathcal{P}_{D_m} = \int_0^{r_D} \mathcal{L}_{I_F}\left(\frac{\gamma_{th} z^{\alpha}}{P_D}\right) \mathcal{L}_{I_{D_m}}\left(\frac{\gamma_{th} z^{\alpha}}{P_D}, z\right) f_{\|\mathbf{x}_{D_{m,o}}\|}(z)\,\mathrm{d}z, \tag{35}$$

where $\mathcal{L}_{I_F}$, $\mathcal{L}_{I_{D_m}}$ and $f_{\|\mathbf{x}_{D_{m,o}}\|}$ are defined in (21), (29) *and* (26), *respectively. When $\Phi_F \sim PPP(\lambda_F)$, the Laplace transform $\mathcal{L}_{I_F}(s)$ is equal to* (27).

Proof. See Appendix B. □

B. F-AP mode

When the user is connected to the closest F-AP located at $\mathbf{x}_{F_{m,o}}$, the SIR γ_{F_m} in (7) is written as

$$\gamma_{F_m} = \frac{P_F g_{F_{m,o}} B_{F,F_{m,o}}^{-\alpha/2}}{I_D + \sum_{k\in\mathbb{N}\setminus\{F_{m,o}\}} P_F g_k B_{F,k}^{-\alpha/2} \Xi_{F,k}}, \tag{36}$$

where $I_D = \sum_{k=1}^{\infty} P_D h_k B_{D,k}^{-\alpha/2} \Xi_{D,k}$. We derive an expression for the coverage probability $\mathcal{P}_{F_m}$ in the following theorem.

Theorem 3. *When the typical user requesting the content c_m is associated with the nearest F-AP which has the content and is within the distance r_F, the coverage probability $\mathcal{P}_{F_m}$ in* (12) *is written as*

$$\mathcal{P}_{F_m} = 2\pi\eta_{F_m}\lambda_F \int_0^{r_F} \mathcal{L}_{I_D}\left(\frac{\gamma_{th} z^{\alpha}}{P_F}\right) \exp\left(-\frac{\pi\lambda_F z^2}{\beta_F}\right) \Upsilon_{F_m}\left(\frac{\pi\lambda_F z^2}{\beta_F}\right) \Delta_{F_m}\left(\frac{\pi\lambda_F z^2}{\beta_F}\right) z\,\mathrm{d}z, \tag{37}$$

where $\mathcal{L}_{I_D}(s)$ is defined in (22) *and for any $x > 0$ we set*

$$\Upsilon_{F_m}(x) = \sum_{i=1}^{\infty} \frac{x^{i-1}}{\Gamma(i)} \left(A_{\eta_{F_m},\beta_F,i}(x, \gamma_{th} x^{\alpha/2})\right)^{-1}, \tag{38}$$

$$\Delta_{F_m}(x) = \prod_{k=1}^{\infty} A_{\eta_{F_m},\beta_F,k}(x, \gamma_{th} x^{\alpha/2}). \tag{39}$$

Here, $A_{\eta_{F_m},\beta_F,i}$ is defined in (34)*. In addition, if $\Phi_D \sim PPP(\lambda_D)$, $\mathcal{L}_{I_D}$ is equal to* (27)*.*

Proof. We omit the proof since it is similar to that of Theorem 1. □

When $\Phi_D \sim PPP(\lambda_D)$ and $\Phi_F \sim PPP(\lambda_F)$, $\mathcal{P}_{F_m}$ is given by the following theorem.

Theorem 4. *When $\Phi_D \sim PPP(\lambda_D)$ and $\Phi_F \sim PPP(\lambda_F)$, the coverage probability $\mathcal{P}_{F_m}$ in* (12) *is expressed as*

$$\mathcal{P}_{F_m} = \int_0^{r_F} \mathcal{L}_{I_{F_m}}\left(\frac{\gamma_{th} z^\alpha}{P_F}, z\right) \mathcal{L}_{I_D}\left(\frac{\gamma_{th} z^\alpha}{P_F}\right) f_{\|\mathbf{x}_{F_m,o}\|}(z)\,\mathrm{d}z, \tag{40}$$

where $\mathcal{L}_{I_{F_m}}$, $\mathcal{L}_{I_D}$ and $f_{\|\mathbf{x}_{F_m,o}\|}$ are defined in (28)*,* (27) *and* (26)*, respectively.*

Proof. We skip the proof as (40) is obtained by proceeding precisely as in the proof of Theorem 2. □

C. Cooperative mode

In the cooperative mode, as can be seen in (10), the desired signal and the interference terms are correlated, and thus it is difficult to derive an exact expression for the coverage probability $\mathcal{P}_C$. To circumvent this difficulty, we neglect the interference $\sum_{\mathbf{x}_k \in \hat{\Phi}_F} P_F g_k \|\mathbf{x}_k\|^{-\alpha}$ since the interferers in $\hat{\Phi}_F$ are located farther than the distance r_C. The SIR γ_C in (10) is consequently approximated as

$$\gamma_C \approx \frac{\sum_{\mathbf{x}_k \in \tilde{\Phi}_F} P_F g_k \|\mathbf{x}_k\|^{-\alpha}}{I_D}. \tag{41}$$

Then, an approximation of the coverage probability $\mathcal{P}_C$ in (13) is given by

$$\begin{aligned}\mathcal{P}_C &\approx \mathbb{P}\left(\frac{\sum_{\mathbf{x}_k \in \tilde{\Phi}_F} P_F g_k \|\mathbf{x}_k\|^{-\alpha}}{I_D} \geq \gamma_{th}\right) = \mathbb{P}\left(Q \geq I_D \gamma_{th}\right) \\ &= \int_0^\infty \mathbb{P}\left(Q \geq x\gamma_{th}\right) f_{I_D}(x)\,\mathrm{d}x = \int_0^\infty \left(1 - F_Q(x\gamma_{th})\right) f_{I_D}(x)\,\mathrm{d}x,\end{aligned} \tag{42}$$

where $Q \triangleq \sum_{\mathbf{x}_k \in \tilde{\Phi}_F} P_F g_k \|\mathbf{x}_k\|^{-\alpha}$. Note that the Laplace transform of I_D is given by (22) and the Laplace transform of Q can be derived as

$$\begin{aligned}\mathcal{L}_Q(s) &= \mathbb{E}\left[\exp\left(-s\sum_{k=1}^\infty P_F g_k B_{F,k}^{-\alpha/2} \Xi_{F,k} \mathbb{1}_{\left\{B_{F,k} \leq r_C^2\right\}}\right)\right] \\ &= \mathbb{E}\left[\prod_{k=1}^\infty \exp\left(-sP_F g_k B_{F,k}^{-\alpha/2} \Xi_{F,k} \mathbb{1}_{\left\{B_{F,k} \leq r_C^2\right\}}\right)\right] = \mathbb{E}\left[\prod_{k=1}^\infty \frac{1}{1 + sP_F B_{F,k}^{-\alpha/2} \Xi_{F,k} \mathbb{1}_{\left\{B_{F,k} \leq r_C^2\right\}}}\right]\end{aligned}$$

$$= \prod_{k=1}^{\infty} \left(\int_0^{\infty} \frac{\beta_F}{1+sP_F x^{-\alpha/2} \mathbb{1}_{\left\{x \le r_C^2\right\}}} f_{B_{F,k}}(x)\,\mathrm{d}x + 1 - \beta_F \right)$$

$$= \prod_{k=1}^{\infty} \left(\int_0^{r_C^2} \frac{\beta_F}{1+sP_F x^{-\alpha/2}} f_{B_{F,k}}(x)\,\mathrm{d}x + \beta_F \int_{r_C^2}^{\infty} f_{B_{F,k}}(x)\,\mathrm{d}x + 1 - \beta_F \right)$$

$$= \prod_{k=1}^{\infty} \left(\int_0^{r_C^2} \frac{\beta_F}{1+sP_F x^{-\alpha/2}} f_{B_{F,k}}(x)\,\mathrm{d}x + 1 - \beta_F \frac{\gamma\left(k, \frac{\pi\lambda_F}{\beta_F} r_C^2\right)}{\Gamma(k)} \right). \tag{43}$$

Note that $F_Q(x)$ and $f_{I_D}(x)$ in (42) can be evaluated by using the inverse Laplace transform (ILT) [35]. For a function F, the ILT is defined as $\mathcal{L}^{-1}\{F\}(x) = \frac{1}{2\pi i} \lim_{T\to\infty} \int_{c-iT}^{c+iT} \exp(sx) F(s)\,\mathrm{d}s$ where $i \triangleq \sqrt{-1}$ and c is a constant. Then, by applying the ILT, we have

$$F_Q(x) = \int_{-\infty}^{x} \mathcal{L}^{-1}\left\{\mathcal{L}_Q(s)\right\}(t)\,\mathrm{d}t = \mathcal{L}^{-1}\left\{\frac{1}{s}\mathcal{L}_Q(s)\right\}(x), \tag{44}$$

$$f_{I_D}(x) = \mathcal{L}^{-1}\left\{\mathcal{L}_{P_{I_D}}(s)\right\}(x). \tag{45}$$

Finally, by substituting (43)-(45) into (42), we obtain an approximation of $\mathcal{P}_C$ in (42). We remark that the ILTs in (44) and (45) can be readily computed by modern techniques, see e.g. [36].

As a special case, when $\Phi_D \sim PPP(\lambda_D)$, $\Phi_F \sim PPP(\lambda_F)$ and $r_C \to \infty$, $F_Q(x)$ and $f_{I_D}(x)$ are expressed in closed-forms as [37]

$$F_Q(x) = 1 - \int_0^{\infty} \frac{1}{\pi u} \exp\left(-ux - \frac{2\pi^2\lambda_F (P_F u)^{2/\alpha}}{\alpha \tan\left(\frac{2\pi}{\alpha}\right)}\right) \sin\left(\frac{2\pi^2\lambda_F (P_F u)^{2/\alpha}}{\alpha}\right) \mathrm{d}u, \tag{46}$$

$$f_{I_D}(x) = \int_0^{\infty} \frac{1}{\pi} \exp\left(-ux - \frac{2\pi^2\lambda_D (P_D u)^{2/\alpha}}{\alpha \tan\left(\frac{2\pi}{\alpha}\right)}\right) \sin\left(\frac{2\pi^2\lambda_D (P_D u)^{2/\alpha}}{\alpha}\right) \mathrm{d}u. \tag{47}$$

Although we can evaluate the approximation of $\mathcal{P}_C$ in (42) using the ILTs with the method in [36], motivated by the fact that $F_Q(x)$ and $f_{I_D}(x)$ have closed-form expressions when $\Phi_D \sim PPP(\lambda_D)$, $\Phi_F \sim PPP(\lambda_F)$ and $r_C \to \infty$, we introduce an approximation of $\mathcal{P}_C$ for the scenario where $\Phi_D \sim PPP(\lambda_D)$ and $\Phi_F \sim GPP(\lambda_F, \beta_F)$, which has a low computational complexity. First, assuming that $r_C \to \infty$ allows us to derive upper-bounds of $F_Q(x)$ when $\Phi_F \sim PPP(\bar{\lambda}_F)$ and $\Phi_F \sim GPP(\lambda_F, \beta_F)$. When $\Phi_F \sim PPP(\bar{\lambda}_F)$, we have

$$F_Q(x) = \mathbb{P}\left(\sum_{k=1}^{\infty} P_F g_k \|\mathbf{x}_k\|^{-\alpha} < x\right) \le \mathbb{P}\left(\forall k \in \mathbb{N}, P_F g_k \|\mathbf{x}_k\|^{-\alpha} < x\right)$$

$$= \mathbb{E}\left[\prod_{k=1}^{\infty} \mathbb{P}\left(g_k \le \frac{x\|\mathbf{x}_k\|^{\alpha}}{P_F}\right)\right] = \mathbb{E}\left[\prod_{k=1}^{\infty} \left(1 - \exp\left(-\frac{x\|\mathbf{x}_k\|^{\alpha}}{P_F}\right)\right)\right]$$

$$= \exp\left(-2\pi\bar{\lambda}_F \int_0^{\infty} \exp\left(-\frac{r^{\alpha}x}{P_F}\right) r\,\mathrm{d}r\right) = \exp\left(-\frac{2\pi\bar{\lambda}_F \Gamma\left(\frac{2}{\alpha}\right)}{\alpha} \left(\frac{P_F}{x}\right)^{2/\alpha}\right). \tag{48}$$

On the other hand, if $\Phi_F \sim GPP(\lambda_F, \beta_F)$, an upper-bound of $F_Q(x)$ is given by

$$\begin{aligned} F_Q(x) &\leq \mathbb{P}\left(\forall k \in \mathbb{N}, P_F g_k \|\mathbf{x}_k\|^{-\alpha} < x\right) = \mathbb{P}\left(\forall k \in \mathbb{N}, P_F g_k B_{F,k}^{-\alpha/2} \Xi_{F,k} < x\right) \\ &= \prod_{k=1}^{\infty} \left(\beta_F \mathbb{P}\left(g_k < \frac{B_{F,k}^{\alpha/2} x}{P_F}\right) + 1 - \beta_F\right) = \prod_{k=1}^{\infty} \left(\beta_F \mathbb{E}\left[1 - \exp\left(-\frac{B_{F,k}^{\alpha/2} x}{P_F}\right)\right] + 1 - \beta_F\right) \\ &= \prod_{k=1}^{\infty} \left(1 - \beta_F \int_0^{\infty} \exp\left(-\frac{u^{\alpha/2} x}{P_F}\right) f_{B_{F,k}}(u)\, \mathrm{d}u\right) \triangleq \bar{F}_Q(x). \end{aligned} \tag{49}$$

We then choose the intensity of the PPP $\bar{\lambda}_F$ which makes the upper-bounds in (48) and (49) equal. By comparing (48) and (49), $\bar{\lambda}_F$ can be identified as

$$\bar{\lambda}_F(x) = \frac{1}{2\pi} \ln\left(\frac{1}{\bar{F}_Q(x)}\right) \frac{\alpha}{\Gamma\left(\frac{2}{\alpha}\right)} \left(\frac{x}{P_F}\right)^{2/\alpha}. \tag{50}$$

Finally, by replacing λ_F in (46) with $\bar{\lambda}_F(x)$ in (50), and by using the results in (42) and (47), we can compute an approximation of $\mathcal{P}_C$ when $\Phi_D \sim PPP(\lambda_D)$ and $\Phi_F \sim GPP(\lambda_F, \beta_F)$ without using the ILTs in (44) and (45). We confirm in our numerical simulations in Fig. 8 that this approximation is tight.

D. Mode selection

In this subsection, we examine the coverage probability for the mode selection algorithm in (16). When $\Phi_D \sim GPP(\lambda_D, \beta_D)$ and $\Phi_F \sim GPP(\lambda_F, \beta_F)$, we derive an expression for $\tilde{\mathcal{P}}_{F_m}$ in (18) in the following theorem.

Theorem 5. *When $\Phi_D \sim GPP(\lambda_D, \beta_D)$ and $\Phi_F \sim GPP(\lambda_F, \beta_F)$, $\tilde{\mathcal{P}}_{F_m}$ in* (18) *is expressed as*

$$\tilde{\mathcal{P}}_{F_m} = 2\pi\eta_{F_m}\lambda_F \int_0^{r_F} \hat{\mathcal{L}}_{I_D}\left(\frac{\gamma_{th} z^{\alpha}}{P_F}\right) \exp\left(-\frac{\pi\lambda_F z^2}{\beta_F}\right) \Upsilon_{F_m}\left(\frac{\pi\lambda_F z^2}{\beta_F}\right) \Delta_{F_m}\left(\frac{\pi\lambda_F z^2}{\beta_F}\right) z\, \mathrm{d}z, \tag{51}$$

where $\Upsilon_{F_m}(z)$ and $\Delta_{F_m}(z)$ are defined in (38) *and* (39)*, respectively. Here,*

$$\begin{aligned} \hat{\mathcal{L}}_{I_D}(\tau) = 2\pi\eta_{D_m}\lambda_D \int_{r_D}^{\infty} &\frac{1}{1 + \tau P_D z^{-\alpha}} \\ &\times \exp\left(-\frac{\pi\lambda_D z^2}{\beta_D}\right) \hat{\Upsilon}_{D_m}\left(\frac{\pi\lambda_D z^2}{\beta_D}, z^2, \tau\right) \hat{\Delta}_{D_m}\left(\frac{\pi\lambda_D z^2}{\beta_D}, z^2, \tau\right) z\, \mathrm{d}z, \end{aligned} \tag{52}$$

$$\hat{\Upsilon}_{D_m}(x, z^2, \tau) = \sum_{q=1}^{\infty} \frac{x^{q-1}}{\Gamma(q)} \left(A_{\eta_{D_m}, \beta_D, q}\left(x, \tau P_D x^{\alpha/2} z^{-\alpha}\right)\right)^{-1}, \tag{53}$$

$$\hat{\Delta}_{D_m}(x, z^2, \tau) = \prod_{l=1}^{\infty} A_{\eta_{D_m}, \beta_D, l}\left(x, \tau P_D x^{\alpha/2} z^{-\alpha}\right), \tag{54}$$

where $A_{\eta_{D_m},\beta_D,q}$ is defined in (34)*. When $\Phi_D \sim PPP(\lambda_D)$, $\hat{\mathcal{L}}_{I_D}$ is given by*

$$\hat{\mathcal{L}}_{I_D}(\tau) = \int_{r_D}^{\infty} \frac{1}{1+\tau P_D z^{-\alpha}} \mathcal{L}_{I_{D_m}}(\tau, z) f_{\|\mathbf{x}_{D_{m,o}}\|}(z)\, \mathrm{d}z. \tag{55}$$

Proof. See Appendix C. □

When $\Phi_D \sim PPP(\lambda_D)$ and $\Phi_F \sim PPP(\lambda_F)$, we compute $\tilde{\mathcal{P}}_{F_m}$ in (18) in the following theorem.

Theorem 6. *When $\Phi_D \sim PPP(\lambda_D)$ and $\Phi_F \sim PPP(\lambda_F)$, $\tilde{\mathcal{P}}_{F_m}$ in* (18) *is given by*

$$\tilde{\mathcal{P}}_{F_m} = \int_0^{r_F} \hat{\mathcal{L}}_{I_D}\left(\frac{\gamma_{th} z^{\alpha}}{P_F}\right) \mathcal{L}_{I_{F_m}}\left(\frac{\gamma_{th} z^{\alpha}}{P_F}, z\right) f_{\|\mathbf{x}_{F_{m,o}}\|}(z)\, \mathrm{d}z, \tag{56}$$

where $\hat{\mathcal{L}}_{I_D}$ and $\mathcal{L}_{I_{F_m}}$ are defined in (55) *and* (28)*, respectively.*

Proof. We omit the proof since the proof is similar to that of Theorem 2. □

Now, we focus on $\tilde{\mathcal{P}}_{C_m}$ in (19). Unlike in the PPP setting, the event $\{\gamma_C \geq \gamma_{th}\}$ is not independent of the events $\{\|\mathbf{x}_{F_{m,o}}\| > r_F\}$ and $\{\|\mathbf{x}_{D_{m,o}}\| > r_D\}$, and therefore it is difficult to obtain an exact expression for $\tilde{\mathcal{P}}_{C_m}$. To overcome this difficulty, we assume that the three events are independent. More precisely, our approximation of $\tilde{\mathcal{P}}_{C_m}$ is given by

$$\begin{aligned}\tilde{\mathcal{P}}_{C_m} &= \mathbb{P}\left(\gamma_C \geq \gamma_{th} \mid \|\mathbf{x}_{F_{m,o}}\| > r_F,\ \|\mathbf{x}_{D_{m,o}}\| > r_D\right) \mathbb{P}\left(\|\mathbf{x}_{F_{m,o}}\| > r_F\right) \mathbb{P}\left(\|\mathbf{x}_{D_{m,o}}\| > r_D\right) \\ &\approx \mathbb{P}\left(\tilde{\gamma}_C \geq \gamma_{th}\right) \left(1 - F_{\|\mathbf{x}_{F_{m,o}}\|}(r_F)\right) \left(1 - F_{\|\mathbf{x}_{D_{m,o}}\|}(r_D)\right), \end{aligned} \tag{57}$$

where $F_{\|\mathbf{x}_{D_{m,o}}\|}(x)$ and $F_{\|\mathbf{x}_{F_{m,o}}\|}(x)$ are defined in (23) and (24), respectively. Here, $\tilde{\gamma}_C \triangleq Q/(\sum_{\mathbf{x}_k \in \hat{\Phi}_F} P_F g_k \|\mathbf{x}_k\|^{-\alpha} + I_D) \approx Q/I_D$ where $Q \triangleq \sum_{\mathbf{x}_k \in \tilde{\Phi}_F} P_F g_k \|\mathbf{x}_k\|^{-\alpha} \mathbb{1}_{\{\|\mathbf{x}_{F_{m,o}}\| > r_F\}}$ and $I_D = \sum_{k=1}^{\infty} P_D h_k B_{D,k}^{-\alpha/2} \Xi_{D,k} \mathbb{1}_{\{\|\mathbf{x}_{D_{m,o}}\| > r_D\}}$. Note that, similarly to (42), we have

$$\mathbb{P}\left(\tilde{\gamma}_C \geq \gamma_{th}\right) \approx \int_0^{\infty} \left(1 - F_Q(x\gamma_{th})\right) f_{I_D}(x)\, \mathrm{d}x. \tag{58}$$

The Laplace transforms of Q and I_D can be respectively represented as

$$\begin{aligned}\mathcal{L}_Q(s) &= \mathbb{E}\left[\prod_{k=1}^{\infty} \left(\frac{\eta_{F_m}\beta_F}{1 + sP_F B_{F,k}^{-\alpha/2} \mathbb{1}_{\left\{r_F^2 < B_{F,k} \leq r_C^2\right\}}} + \frac{(1-\eta_{F_m})\beta_F}{1 + sP_F B_{F,k}^{-\alpha/2} \mathbb{1}_{\left\{B_{F,k} \leq r_C^2\right\}}} + 1 - \beta_F\right)\right] \\ &= \prod_{k=1}^{\infty} \left(\int_0^{\infty} \frac{\eta_{F_m}\beta_F}{1 + sP_F x^{-\alpha/2} \mathbb{1}_{\left\{r_F^2 < x \leq r_C^2\right\}}} f_{B_{F,k}}(x)\, \mathrm{d}x + \int_0^{\infty} \frac{(1-\eta_{F_m})\beta_F}{1 + sP_F x^{-\alpha/2} \mathbb{1}_{\left\{x \leq r_C^2\right\}}} f_{B_{F,k}}(x)\, \mathrm{d}x + 1 - \beta_F\right) \\ &= \prod_{k=1}^{\infty} \left(\int_{r_F^2}^{r_C^2} \frac{\eta_{F_m}\beta_F}{1 + sP_F x^{-\alpha/2}} f_{B_{F,k}}(x)\, \mathrm{d}x + \int_0^{r_C^2} \frac{(1-\eta_{F_m})\beta_F}{1 + sP_F x^{-\alpha/2}} f_{B_{F,k}}(x)\, \mathrm{d}x\right. \end{aligned}$$

TABLE II

SYSTEM PARAMETERS

Symbol	r_D	r_F	r_C	β_D	β_F	P_D	P_F	M	α
Value	15 m	100 m	500 m	1	1	3 dBm	23 dBm	100	4

$$+1-\frac{\beta_F}{\Gamma(k)}\left(\gamma\left(k,\frac{\pi\lambda_F}{\beta_F}r_C^2\right)-\eta_{F_m}\gamma\left(k,\frac{\pi\lambda_F}{\beta_F}r_F^2\right)\right)\Bigg), \tag{59}$$

$$\begin{aligned}\mathcal{L}_{I_D}(s)&=\mathbb{E}\left[\prod_{k=1}^{\infty}\left(\frac{\eta_{D_m}\beta_D}{1+sP_DB_{D,k}^{-\alpha/2}\mathbb{1}_{\left\{r_D^2<B_{D,k}\right\}}}+\frac{(1-\eta_{D_m})\beta_D}{1+sP_DB_{D,k}^{-\alpha/2}}+1-\beta_D\right)\right]\\&=\prod_{k=1}^{\infty}\Bigg(\int_{r_D^2}^{\infty}\frac{\eta_{D_m}\beta_D}{1+sP_Dx^{-\alpha/2}}f_{B_{D,k}}(x)\,\mathrm{d}x+\int_0^{\infty}\frac{(1-\eta_{D_m})\beta_F}{1+sP_Dx^{-\alpha/2}}f_{B_{D,k}}(x)\,\mathrm{d}x\\&\qquad+1-\beta_D+\frac{\eta_{D_m}\beta_D\gamma\left(k,\frac{\pi\lambda_D}{\beta_D}r_D^2\right)}{\Gamma(k)}\Bigg).\end{aligned} \tag{60}$$

By adopting the ILTs in (44) and (45), $\tilde{\mathcal{P}}_{C_m}$ in (57) can be evaluated.

IV. SIMULATION RESULTS

In this section, we illustrate numerical simulation results to validate our analysis. In Figs. 2-10, the lines and symbols are used to indicate the analytical and simulated results, respectively. For brevity of presentation, we denote by the networks with PPP distributed D2D transmitters and β-GPP distributed F-APs as *PPP-GPP*. Also, *PPP-PPP* and *GPP-GPP* are defined in the same manner. Unless otherwise stated, we use the network parameters listed in Table II.

Figs. 2-4 exhibit the coverage probability for the D2D mode when $\lambda_F = 5\times10^{-4}$. In Fig. 2, we evaluate the coverage probability $\mathcal{P}_{D_m}$ in (31) when $\lambda_D = 0.01$ and $\eta_{D_m} = 1$. We observe that $\mathcal{P}_{D_m}$ is a decreasing function of γ_{th}. Also, $\mathcal{P}_{D_m}$ increases when r_D grows as the probability that there exist D2D transmitters having the accessed content becomes higher when r_D gets larger. Since a growth of the degree of repulsion results in a decrease of the contact distance, $\mathcal{P}_{D_m}$ is enhanced when the distribution of the D2D transmitters follows a β-GPP. In addition, it is shown that the impact of the distribution of the F-APs is marginal when $r_D = 5$ and 7 m since $\mathcal{P}_{D_m}$ is dominated by the signal from the associated D2D transmitter when r_D is small.

Fig. 3 plots $\mathcal{P}_{D_m}$ in (31) in networks with $\gamma_{th} = -15$ dB. First, we see that $\mathcal{P}_{D_m}$ is an increasing function of λ_D and η_{D_m} as the intensity of the D2D transmitters caching the requested content is equal to $\lambda_D\eta_{D_m}$. Note that $\mathcal{P}_{D_m}$ becomes lower when the spatial distribution of the F-APs is

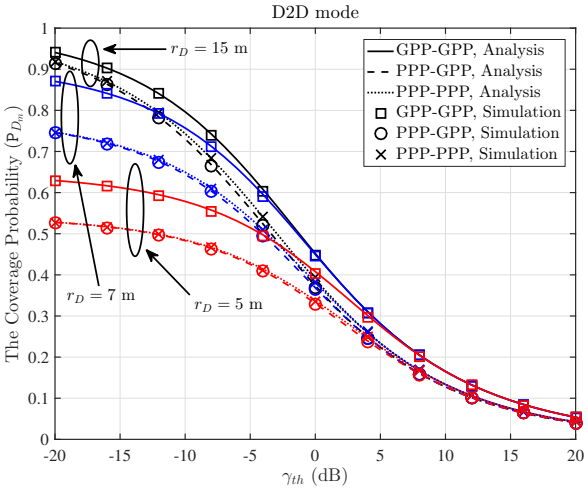

Fig. 2. Coverage probability for the D2D mode $\mathcal{P}_{D_m}$ as a function of γ_{th}.

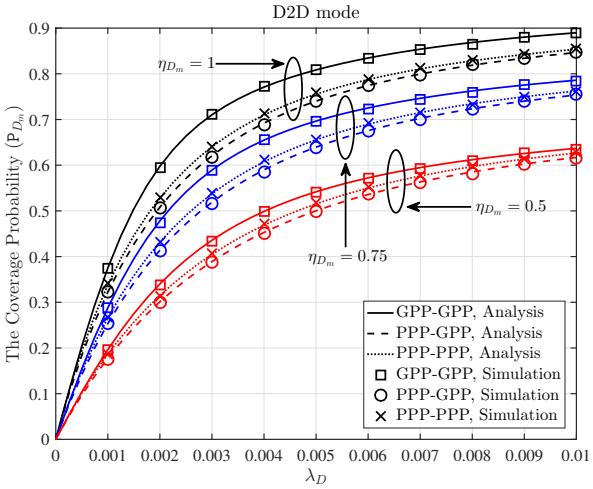

Fig. 3. Coverage probability for the D2D mode $\mathcal{P}_{D_m}$ as a function of λ_D.

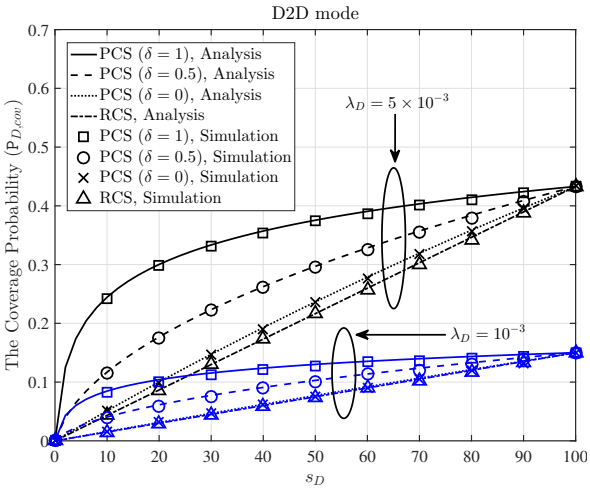

Fig. 4. Average coverage probability for the D2D mode $\mathcal{P}_{D,cov}$ as a function of s_D.

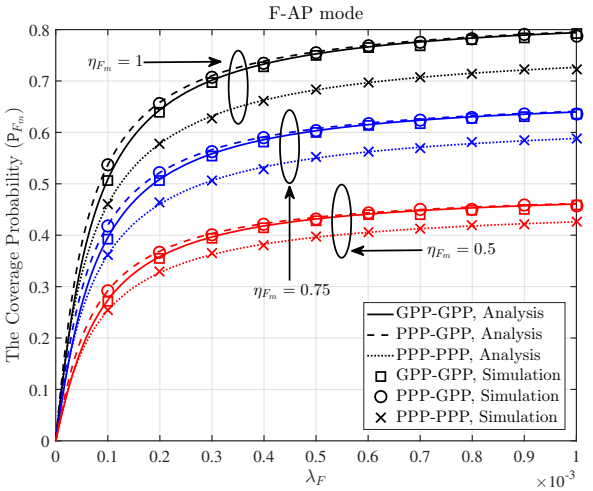

Fig. 5. Coverage probability for the F-AP mode $\mathcal{P}_{F_m}$ as a function of λ_F.

a β-GPP. This is due to the fact that the probability that interfering F-APs are located near the typical user gets higher when there exists repulsion among the locations of the F-APs. Moreover, it is observed that the influence of β_D decreases as η_{D_m} decays.

The average coverage probability $\mathcal{P}_{D,cov}$ in (14) for PPP-GPP networks is examined in Fig. 4 when $\gamma_{th} = -5$ dB. Since the intensity of the D2D transmitters having the accessed content grows as λ_D and s_D become bigger, $\mathcal{P}_{D,cov}$ decreases as λ_D and s_D get smaller. Also, an increase in δ leads to a growth of $\{\eta_{D_m}\}$, and therefore $\mathcal{P}_{D,cov}$ is an increasing function of δ. Moreover, by comparing the cases “PCS ($\delta = 0$)" and “RCS", we can infer that a higher $\mathcal{P}_{D,cov}$ can be achieved

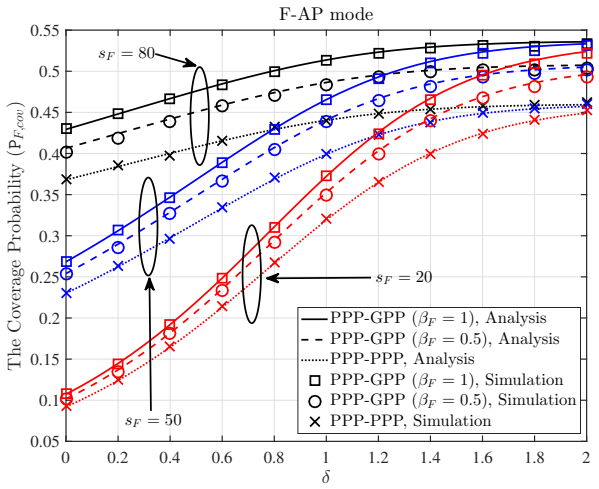

Fig. 6. Average coverage probability for the F-AP mode $\mathcal{P}_{F,cov}$ as a function of δ.

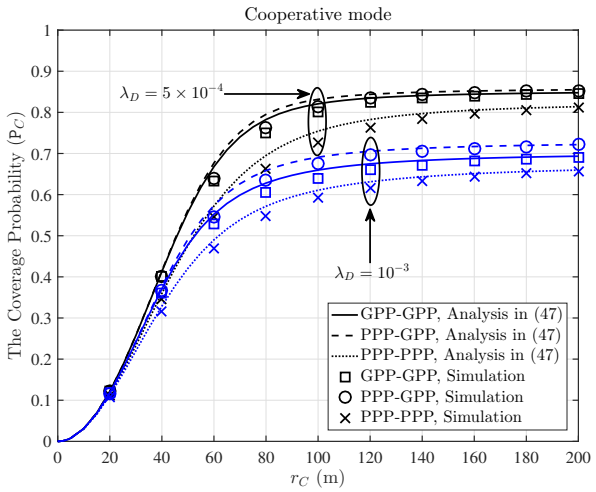

Fig. 7. Coverage probability for the cooperative mode $\mathcal{P}_C$ as a function of r_C.

by employing the PCS even when the content popularity follows the uniform distribution.

Figs. 5 and 6 present the coverage probability for the F-AP mode when $\lambda_D = 10^{-3}$ and $\gamma_{th} = -5$ dB. In Fig. 5, we plot the coverage probability $\mathcal{P}_{F_m}$ in (37) for various values of η_{F_m}. As λ_F and η_{F_m} grow, the probability that there exist F-APs caching the requested content becomes larger and the contact distance decreases, and hence $\mathcal{P}_{F_m}$ is an increasing function of λ_F and η_{F_m}. We remark that the interference from the F-APs gets bigger as λ_F increases. From the observation that $\mathcal{P}_{F_m}$ is increased with λ_F, we deduce that the impact of the contact distance is more pronounced than that of the interference. In addition, since the contact distance gets smaller if there exists repulsion among the locations of the F-APs, $\mathcal{P}_{F_m}$ is enhanced when Φ_F follows a β-GPP.

Fig. 6 evaluates the average coverage probability for the F-AP mode $\mathcal{P}_{F,cov}$ in (15) for the networks where the locations of the D2D transmitters follow a PPP, $\lambda_F = 10^{-4}$ and the PCS strategy in (2) is employed. Since increases in s_F and δ lead to a growth of the intensity of Φ_{F_m}, $\mathcal{P}_{F,cov}$ decays as s_F and δ become lower. As expected, $\mathcal{P}_{F,cov}$ increases as β_F goes to one. It is shown that $\mathcal{P}_{F,cov}$ is sensitive to δ when s_F is small. Also, the coverage probabilities with different values of s_F converge as δ increases since a small number of contents are frequently requested by users when δ is large.

In Figs. 7 and 8, we illustrate the coverage probability for the cooperative mode $\mathcal{P}_C$ in (13). Fig. 7 establishes $\mathcal{P}_C$ for the networks with $\lambda_F = 10^{-4}$ and $\gamma_{th} = -5$ dB for different values of

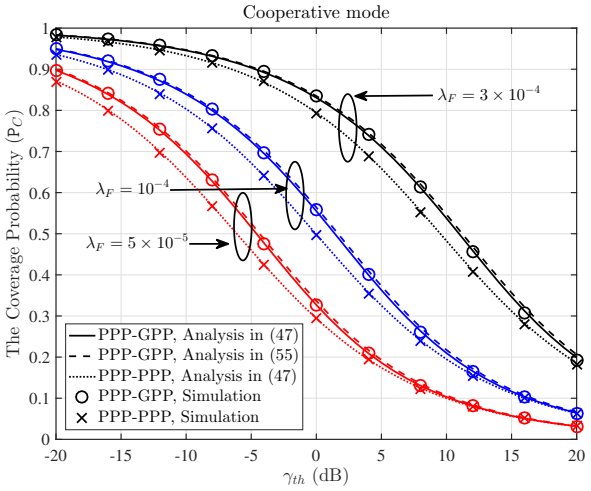

Fig. 8. Coverage probability for the cooperative mode $\mathcal{P}_C$ as a function of γ_{th}.

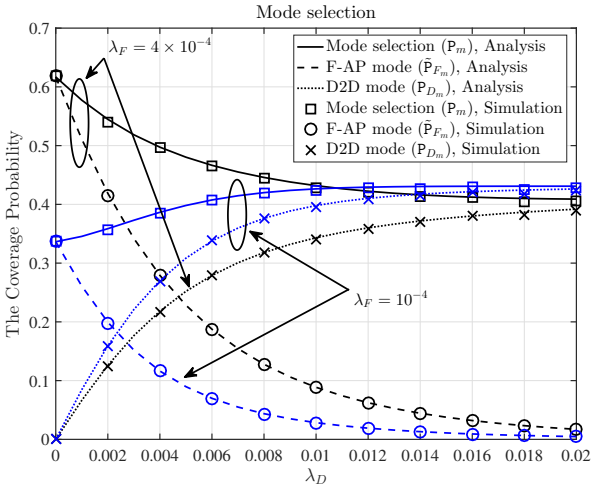

Fig. 9. Coverage probability for the mode selection algorithm as a function of λ_D.

r_C. Note that our approximation in (42) is tight when $r_C \geq 150$ m, which is a practical case. The coverage probability $\mathcal{P}_C$ decreases as λ_D increases since a higher λ_D results in a bigger interference. In Fig. 8, we exhibit the coverage probability for the cooperative mode $\mathcal{P}_C$ for networks with $\lambda_D = 10^{-3}$. It is shown that our approximation of $\mathcal{P}_C$ for PPP-GPP networks using (50) is accurate for various values of γ_{th} and λ_F. Moreover, we see from Figs. 7 and 8 that $\mathcal{P}_C$ decreases as the repulsion among the locations of the F-APs (or D2D transmitters) reduces (or grows).

Figs. 9 and 10 examine the coverage probability for the mode selection algorithm when $r_D = 10$ m, $r_F = 50$ m, $s_D = 30$ and $s_F = 50$. In Fig. 9, we demonstrate the coverage probability $\mathcal{P}_m$ in (17) for GPP-GPP networks where the RCS in (1) is adopted and $\gamma_{th} = -10$ dB. In Fig. 9, we consider the case where a typical user selects one of the D2D and the F-AP modes, and therefore the coverage probability $\mathcal{P}_m$ in (17) is $\mathcal{P}_m = \mathcal{P}_{D_m} + \tilde{\mathcal{P}}_{F_m}$. First of all, it is confirmed that our analysis for $\tilde{\mathcal{P}}_{F_m}$ in (51) is valid. In addition, we observe that $\tilde{\mathcal{P}}_{F_m}$ is increasing and decreasing functions of λ_F and λ_D, respectively. A similar interpretation can be made for $\mathcal{P}_{D_m}$. An important point to note here is the fact that the trends of $\mathcal{P}_m$ with respect to λ_D for the cases with $\lambda_F = 10^{-4}$ and $\lambda_F = 4 \times 10^{-4}$ are different. More specifically, when $\lambda_F = 10^{-4}$ (or $\lambda_F = 4 \times 10^{-4}$), $\mathcal{P}_m$ grows (or decays) as λ_D becomes larger. This phenomenon can be explained by the fact that $\mathcal{P}_{D_m}$ (or $\tilde{\mathcal{P}}_{F_m}$) dominates $\mathcal{P}_m$ when λ_F is low (or high).

Fig. 10 evaluates the coverage probability $\mathcal{P}_{cov}$ in (16) for the PPP-GPP networks where

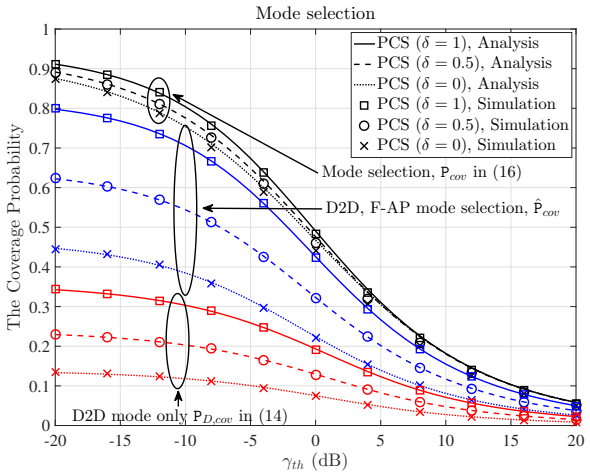

Fig. 10. Coverage probability for the mode selection algorithm as a function of γ_{th}.

the PCS in (2) is employed, $\lambda_D = 2 \times 10^{-3}$ and $\lambda_F = 2 \times 10^{-4}$. Here, we define $\hat{\mathcal{P}}_{cov}$ as $\hat{\mathcal{P}}_{cov} \triangleq \sum_{m=1}^{M} \xi_m (\mathcal{P}_{D_m} + \tilde{\mathcal{P}}_{F_m})$ which indicates the coverage probability for the case where the typical user selects one of the D2D and the F-AP modes. In Fig. 10, it is shown that the approximation in (57) exhibits only negligible gaps compared to the simulated results. Also, we see that by employing the mode selection algorithm, a high coverage probability can be achieved, which is insensitive to δ. For example, when δ is low, the probability that there is no D2D transmitter or F-AP having the accessed content increases, and therefore the user is more likely to choose the cooperative mode. As a result, although $\mathcal{P}_{D,cov}$ and $\hat{\mathcal{P}}_{cov}$ with $\delta = 0$ are smaller than those with $\delta = 1$, $\mathcal{P}_{cov}$ with $\delta = 0$ is almost identical to that with $\delta = 1$.

V. Conclusion

In this paper, we have studied F-RANs where the locations of D2D transmitters and F-APs are modeled as β-GPPs in order to reflect the repulsive nature of the networks. We have considered three types of access modes, namely D2D, F-AP and cooperative modes. In the D2D and the F-AP modes, requested contents are delivered by exploiting the proactive caching. In the cooperative mode, data is transferred by leveraging a cloud processing. We have analyzed the coverage probabilities for the three modes. Additionally, we have examined the coverage probability of the mode selection algorithm which judiciously selects one of the three mode and takes full advantage of the centralized processing and the edge caching. Numerical simulations have verified the accuracy of our analytical results.

APPENDIX A
PROOF OF THEOREM 1

We begin by defining a sequence of discrete random variables $\{\epsilon_{D,i}\}_{i\in\mathbb{N}}$ which are independent marks of Φ_D such that $\epsilon_{D,i} \in \{0,1\}$ and $\mathbb{P}(\epsilon_{D,i}=1) = \eta_{D_m}$. Here, $\{\epsilon_{D,i}=1\}$ and $\{\epsilon_{D,i}=0\}$ are the events wherein the D2D transmitter at $\mathbf{x}_i$ has the content c_m and does not have it, respectively. For any $i \in \mathbb{N}$, we set

$$I_i := \bigcap_{k\in\mathbb{N}\setminus\{i\}} \big\{B_{D,k} \geq B_{D,i} \text{ or } \epsilon_{D,k}=0 \text{ or } \Xi_{D,k}=0\big\},$$

as well as

$$J_i := I_i \cap \{\epsilon_{D,i}=1\} \cap \{\Xi_{D,i}=1\},$$

and it is easy to check that the events $\{J_i\}_{i\in\mathbb{N}}$ are disjoint almost surely. Additionally, on the event J_i we have $\|\mathbf{x}_{D_{m,o}}\|^2 = B_{D,i}$. Consequently, we have

$$\begin{aligned}
\mathcal{P}_{D_m} &\triangleq \mathbb{P}\big(\gamma_{D_m} \geq \gamma_{th}, \|\mathbf{x}_{D_{m,o}}\| \leq r_D\big) \\
&= \sum_{i=1}^{\infty} \mathbb{P}\big(\gamma_{D_m} \geq \gamma_{th},\ B_{D,i} \leq r_D^2,\ \epsilon_{D,i}=1,\ \Xi_{D,i}=1,\ I_i\big) \\
&= \sum_{i=1}^{\infty} \mathbb{P}\left(\frac{P_D h_i B_{D,i}^{-\alpha/2}}{\sum_{k\in\mathbb{N}\setminus\{i\}} P_D h_k B_{D,k}^{-\alpha/2}\Xi_{D,k} + I_F} \geq \gamma_{th},\ B_{D,i} \leq r_D^2,\ \epsilon_{D,i}=1,\ \Xi_{D,i}=1,\ I_i\right) \qquad (61) \\
&= \sum_{i=1}^{\infty} \mathbb{P}\left(h_i \geq \frac{\gamma_{th} B_{D,i}^{\alpha/2}}{P_D}\left(\sum_{k\in\mathbb{N}\setminus\{i\}} P_D h_k B_{D,k}^{-\alpha/2}\Xi_{D,k} + I_F\right),\ B_{D,i} \leq r_D^2,\ I_i\right) \\
&\qquad \times \mathbb{P}(\epsilon_{D,i}=1,\ \Xi_{D,i}=1) \\
&= \eta_{D_m}\beta_D \sum_{i=1}^{\infty} \mathbb{E}\left[\exp\left(-\frac{\gamma_{th} B_{D,i}^{\alpha/2}}{P_D}\left(\sum_{k\in\mathbb{N}\setminus\{i\}} P_D h_k B_{D,k}^{-\alpha/2}\Xi_{D,k} + I_F\right)\right)\mathbb{1}_{\left\{B_{D,i}\leq r_D^2,\ I_i\right\}}\right] \\
&= \eta_{D_m}\beta_D \sum_{i=1}^{\infty} \mathbb{E}\left[\mathcal{L}_{I_F}\left(\frac{\gamma_{th} B_{D,i}^{\alpha/2}}{P_D}\right)\prod_{k\in\mathbb{N}\setminus\{i\}} \exp\left(-\gamma_{th} B_{D,i}^{\alpha/2} h_k B_{D,k}^{-\alpha/2}\Xi_{D,k}\right)\mathbb{1}_{\left\{B_{D,i}\leq r_D^2,\ I_i\right\}}\right] \\
&= \eta_{D_m}\beta_D \sum_{i=1}^{\infty} \mathbb{E}\Bigg[\mathcal{L}_{I_F}\left(\frac{\gamma_{th} B_{D,i}^{\alpha/2}}{P_D}\right)\mathbb{1}_{\left\{B_{D,i}\leq r_D^2\right\}} \\
&\qquad \times \prod_{k\in\mathbb{N}\setminus\{i\}}\left[\frac{1}{1+\gamma_{th} B_{D,i}^{\alpha/2} B_{D,k}^{-\alpha/2}\Xi_{D,k}}\mathbb{1}_{\left\{B_{D,k}\geq B_{D,i} \text{ or } \epsilon_{D,k}=0 \text{ or } \Xi_{D,k}=0\right\}}\right]\Bigg]
\end{aligned}$$

$$= \eta_{D_m}\beta_D \sum_{i=1}^{\infty} \mathbb{E}\Bigg[\mathcal{L}_{I_F}\left(\frac{\gamma_{th}B_{D,i}^{\alpha/2}}{P_D}\right)\mathbb{1}_{\left\{B_{D,i}\le r_D^2\right\}} \times \prod_{k\in\mathbb{N}\setminus\{i\}}\left[\frac{1}{1+\gamma_{th}B_{D,i}^{\alpha/2}B_{D,k}^{-\alpha/2}\Xi_{D,k}}\left(\mathbb{1}_{\left\{\Xi_{D,k}=1\right\}}\mathbb{1}_{\left\{B_{D,k}\ge B_{D,i} \text{ or } \epsilon_{D,k}=0\right\}} + \mathbb{1}_{\left\{\Xi_{D,k}=0\right\}}\right)\right]\Bigg]$$

$$= \eta_{D_m}\beta_D \sum_{i=1}^{\infty} \mathbb{E}\Bigg[\mathcal{L}_{I_F}\left(\frac{\gamma_{th}B_{D,i}^{\alpha/2}}{P_D}\right)\mathbb{1}_{\left\{B_{D,i}\le r_D^2\right\}} \times \prod_{k\in\mathbb{N}\setminus\{i\}}\left[1-\beta_D+\frac{\beta_D}{1+\gamma_{th}B_{D,i}^{\alpha/2}B_{D,k}^{-\alpha/2}}\mathbb{1}_{\left\{B_{D,k}\ge B_{D,i} \text{ or } \epsilon_{D,k}=0\right\}}\right]\Bigg]. \tag{62}$$

We remark that $\mathbb{1}_{\{B_{D,k}\ge B_{D,i} \text{ or } \epsilon_{D,i}=0\}} = \mathbb{1}_{\{B_{D,k}\ge B_{D,i} \text{ and } \epsilon_{D,i}=1\}} + \mathbb{1}_{\{\epsilon_{D,i}=0\}}$, and therefore $\mathcal{P}_{D_m}$ in (62) is computed as

$$\begin{aligned}
\mathcal{P}_{D_m} &= \eta_{D_m}\beta_D \sum_{i=1}^{\infty} \mathbb{E}\Bigg[\mathcal{L}_{I_F}\left(\frac{\gamma_{th}B_{D,i}^{\alpha/2}}{P_D}\right)\mathbb{1}_{\left\{B_{D,i}\le r_D^2\right\}} \times \prod_{k\in\mathbb{N}\setminus\{i\}}\left[1-\beta_D+\frac{\eta_{D_m}\beta_D}{1+\gamma_{th}B_{D,i}^{\alpha/2}B_{D,k}^{-\alpha/2}}\mathbb{1}_{\left\{B_{D,k}\ge B_{D,i}\right\}}+\frac{(1-\eta_{D_m})\beta_D}{1+\gamma_{th}B_{D,i}^{\alpha/2}B_{D,k}^{-\alpha/2}}\right]\Bigg] \\
&= \eta_{D_m}\beta_D \sum_{i=1}^{\infty} \int_0^{r_D^2} \mathcal{L}_{I_F}\left(\frac{\gamma_{th}u^{\alpha/2}}{P_D}\right) f_{B_{D,i}}(u) \prod_{k\in\mathbb{N}\setminus\{i\}}\Bigg(1-\beta_D \\
&\quad + \int_u^{\infty} \frac{\eta_{D_m}\beta_D}{1+\gamma_{th}u^{\alpha/2}x^{-\alpha/2}} f_{B_{D,k}}(x)\,\mathrm{d}x + \int_0^{\infty} \frac{(1-\eta_{D_m})\,\beta_D}{1+\gamma_{th}u^{\alpha/2}x^{-\alpha/2}} f_{B_{D,k}}(x)\,\mathrm{d}x\Bigg)\,\mathrm{d}u \\
&= 2\eta_{D_m}\beta_D \sum_{i=1}^{\infty} \int_0^{r_D} \mathcal{L}_{I_F}\left(\frac{\gamma_{th}z^{\alpha}}{P_D}\right) f_{B_{D,i}}(z^2) \prod_{k\in\mathbb{N}\setminus\{i\}}\Bigg(1-\beta_D \\
&\quad + \int_{z^2}^{\infty} \frac{\eta_{D_m}\beta_D}{1+\gamma_{th}z^{\alpha}x^{-\alpha/2}} f_{B_{D,k}}(x)\,\mathrm{d}x + \int_0^{\infty} \frac{(1-\eta_{D_m})\,\beta_D}{1+\gamma_{th}z^{\alpha}x^{-\alpha/2}} f_{B_{D,k}}(x)\,\mathrm{d}x\Bigg) z\,\mathrm{d}z.
\end{aligned} \tag{63}$$

Here, by (20) and a change of variable, the inner integral terms in (63) can be rewritten as

$$\int_{z^2}^{\infty} \frac{\eta_{D_m}\beta_D}{1+\gamma_{th}z^{\alpha}x^{-\alpha/2}} f_{B_{D,k}}(x)\,\mathrm{d}x = \int_{\pi\lambda_D z^2/\beta_D}^{\infty} \frac{\eta_{D_m}\beta_D\nu^{k-1}\exp(-\nu)}{\Gamma(k)\left(1+\gamma_{th}\left(\frac{\pi\lambda_D z^2}{\beta_D}\right)^{\alpha/2}\nu^{-\alpha/2}\right)}\,\mathrm{d}\nu, \tag{64}$$

$$\int_0^{\infty} \frac{(1-\eta_{D_m})\,\beta_D}{1+\gamma_{th}z^{\alpha}x^{-\alpha/2}} f_{B_{D,k}}(x)\,\mathrm{d}x = \int_0^{\infty} \frac{(1-\eta_{D_m})\,\beta_D\nu^{k-1}\exp(-\nu)}{\Gamma(k)\left(1+\gamma_{th}\left(\frac{\pi\lambda_D z^2}{\beta_D}\right)^{\alpha/2}\nu^{-\alpha/2}\right)}\,\mathrm{d}\nu. \tag{65}$$

By plugging (64) and (65) into (63), we obtain

$$\mathcal{P}_{D_m} = 2\pi\eta_{D_m}\lambda_D \sum_{i=1}^{\infty} \int_0^{r_D} \mathcal{L}_{I_F}\left(\frac{\gamma_{th}z^{\alpha}}{P_D}\right) \frac{\left(\frac{\pi\lambda_D z^2}{\beta_D}\right)^{i-1}\exp\left(-\frac{\pi\lambda_D z^2}{\beta_D}\right)}{\Gamma(i)}$$

$$\times \prod_{k\in\mathbb{N}\setminus\{i\}} \left(1-\beta_D+\int_{\pi\lambda_D z^2/\beta_D}^{\infty} \frac{\eta_{D_m}\beta_D\nu^{k-1}\exp(-\nu)}{\Gamma(k)\left(1+\gamma_{th}\left(\frac{\pi\lambda_D z^2}{\beta_D}\right)^{\alpha/2}\nu^{-\alpha/2}\right)}\,\mathrm{d}\nu \right.$$
$$\left. +\int_0^{\infty} \frac{(1-\eta_{D_m})\,\beta_D\nu^{k-1}\exp(-\nu)}{\Gamma(k)\left(1+\gamma_{th}\left(\frac{\pi\lambda_D z^2}{\beta_D}\right)^{\alpha/2}\nu^{-\alpha/2}\right)}\,\mathrm{d}\nu\right) z\,\mathrm{d}z,$$

which concludes the proof.

APPENDIX B
PROOF OF THEOREM 2

The aim of the proof is to compute the limit of (31) as β_D goes to zero. First, note that for any $x>0$ we have

$$0\le\int_x^{\infty}\frac{\eta_{D_m}\beta_D\nu^{k-1}\exp(-\nu)}{\Gamma(k)\,(1+\gamma_{th}x^{\alpha/2}\nu^{-\alpha/2})}\,\mathrm{d}\nu\le\int_0^{\infty}\frac{\eta_{D_m}\beta_D\nu^{k-1}\exp(-\nu)}{\Gamma(k)}\,\mathrm{d}\nu=\eta_{D_m}\beta_D, \tag{66}$$

and similarly

$$0\le\int_0^{\infty}\frac{(1-\eta_{D_m})\beta_D\nu^{i-1}\exp(-\nu)}{\Gamma(i)\,(1+\gamma_{th}x^{\alpha/2}\nu^{-\alpha/2})}\,\mathrm{d}\nu\le(1-\eta_{D_m})\beta_D. \tag{67}$$

Thus, taking $x=\pi\lambda_D z^2/\beta_D$ we obtain

$$1\le\exp\left(-\frac{\pi\lambda_D z^2}{\beta_D}\right)\Upsilon_{D_m}\left(\frac{\pi\lambda_D z^2}{\beta_D}\right)\le(1-\beta_D)^{-1}, \tag{68}$$

which implies

$$\exp\left(-\frac{\pi\lambda_D z^2}{\beta_D}\right)\Upsilon_{D_m}\left(\frac{\pi\lambda_D z^2}{\beta_D}\right)\xrightarrow[\beta_D\to 0]{}1. \tag{69}$$

Second, let us fix $\varepsilon>0$ and $x>0$. By (66) and (67), for any $k\ge 1$ we have

$$0\le\beta_D-\int_{x/\beta_D}^{\infty}\frac{\eta_{D_m}\beta_D\nu^{k-1}\exp(-\nu)}{\Gamma(k)\,(1+\gamma_{th}x^{\alpha/2}(\nu\beta_D)^{-\alpha/2})}\,\mathrm{d}\nu-\int_0^{\infty}\frac{(1-\eta_{D_m})\beta_D\nu^{k-1}\exp(-\nu)}{\Gamma(k)\,(1+\gamma_{th}x^{\alpha/2}(\nu\beta_D)^{-\alpha/2})}\,\mathrm{d}\nu\le\beta_D, \tag{70}$$

and additionally we note that

$$\beta_D-\int_{x/\beta_D}^{\infty}\frac{\eta_{D_m}\beta_D\nu^{k-1}\exp(-\nu)}{\Gamma(k)\,(1+\gamma_{th}x^{\alpha/2}(\nu\beta_D)^{-\alpha/2})}\,\mathrm{d}\nu-\int_0^{\infty}\frac{(1-\eta_{D_m})\beta_D\nu^{k-1}\exp(-\nu)}{\Gamma(k)\,(1+\gamma_{th}x^{\alpha/2}(\nu\beta_D)^{-\alpha/2})}\,\mathrm{d}\nu$$
$$=\int_0^{x/\beta_D}\frac{\eta_{D_m}\beta_D\nu^{k-1}\exp(-\nu)}{\Gamma(k)\,(1+\gamma_{th}x^{\alpha/2}(\nu\beta_D)^{-\alpha/2})}\,\mathrm{d}\nu+\int_0^{\infty}\frac{\beta_D\nu^{k-1}\exp(-\nu)}{\Gamma(k)\,(1+(\nu\beta_D)^{\alpha/2}x^{-\alpha/2}/\gamma_{th})}\,\mathrm{d}\nu. \tag{71}$$

For x sufficiently small, the inequalities $-(1+\varepsilon)x\le\ln(1-x)\le-x$ hold, and therefore by (70) and (71), for β_D sufficiently small we have

$$-(1+\varepsilon)\left(\int_0^{x/\beta_D}\frac{\eta_{D_m}\beta_D\nu^{k-1}\exp(-\nu)}{\Gamma(k)\,(1+\gamma_{th}x^{\alpha/2}(\nu\beta_D)^{-\alpha/2})}\,\mathrm{d}\nu+\int_0^{\infty}\frac{\beta_D\nu^{k-1}\exp(-\nu)}{\Gamma(k)\,(1+(\nu\beta_D)^{\alpha/2}x^{-\alpha/2}/\gamma_{th})}\,\mathrm{d}\nu\right)$$

$$\leq \ln\bigg(1-\beta_D+\int_{x/\beta_D}^{\infty}\frac{\eta_{D_m}\beta_D\nu^{k-1}\exp(-\nu)}{\Gamma(k)\,(1+\gamma_{th}x^{\alpha/2}(\nu\beta_D)^{-\alpha/2})}\,\mathrm{d}\nu+\int_0^{\infty}\frac{(1-\eta_{D_m})\beta_D\nu^{k-1}\exp(-\nu)}{\Gamma(k)\,(1+\gamma_{th}x^{\alpha/2}(\nu\beta_D)^{-\alpha/2})}\,\mathrm{d}\nu\bigg)$$

$$\leq -\int_0^{x/\beta_D}\frac{\eta_{D_m}\beta_D\nu^{k-1}\exp(-\nu)}{\Gamma(k)\,(1+\gamma_{th}x^{\alpha/2}(\nu\beta_D)^{-\alpha/2})}\,\mathrm{d}\nu-\int_0^{\infty}\frac{\beta_D\nu^{k-1}\exp(-\nu)}{\Gamma(k)\,(1+(\nu\beta_D)^{\alpha/2}x^{-\alpha/2}/\gamma_{th})}\,\mathrm{d}\nu,$$

for all $k\geq 1$. We deduce from the above inequalities that for β_D sufficiently small the following holds:

$$\exp\bigg(-(1+\varepsilon)\bigg(\int_0^{x/\beta_D}\frac{\eta_{D_m}\beta_D\,\mathrm{d}\nu}{1+\gamma_{th}x^{\alpha/2}(\nu\beta_D)^{-\alpha/2}}+\int_0^{\infty}\frac{\beta_D\,\mathrm{d}\nu}{1+(\nu\beta_D)^{\alpha/2}x^{-\alpha/2}/\gamma_{th}}\bigg)\bigg)\leq\Delta_{D_m}\bigg(\frac{x}{\beta_D}\bigg)$$
$$\leq\exp\bigg(-\int_0^{x/\beta_D}\frac{\eta_{D_m}\beta_D}{1+\gamma_{th}x^{\alpha/2}(\nu\beta_D)^{-\alpha/2}}\,\mathrm{d}\nu-\int_0^{\infty}\frac{\beta_D}{1+(\nu\beta_D)^{\alpha/2}x^{-\alpha/2}/\gamma_{th}}\,\mathrm{d}\nu\bigg),$$

and so by change of variable,

$$\exp\bigg(-(1+\varepsilon)\bigg(\int_0^{x}\frac{\eta_{D_m}\,\mathrm{d}y}{1+\gamma_{th}x^{\alpha/2}y^{-\alpha/2}}+\int_0^{\infty}\frac{\mathrm{d}y}{1+y^{\alpha/2}x^{-\alpha/2}/\gamma_{th}}\bigg)\bigg)\leq\Delta_{D_m}\bigg(\frac{x}{\beta_D}\bigg)$$
$$\leq\exp\bigg(-\int_0^{x}\frac{\eta_{D_m}\,\mathrm{d}y}{1+\gamma_{th}x^{\alpha/2}y^{-\alpha/2}}-\int_0^{\infty}\frac{\mathrm{d}y}{1+y^{\alpha/2}x^{-\alpha/2}/\gamma_{th}}\bigg).\quad(72)$$

Since the above is true for all $\varepsilon>0$, we obtain

$$\Delta_{D_m}\bigg(\frac{x}{\beta_D}\bigg)\xrightarrow[\beta_D\to 0]{}\exp\bigg(-\int_0^{x}\frac{\eta_{D_m}\,\mathrm{d}y}{1+\gamma_{th}x^{\alpha/2}y^{-\alpha/2}}-\int_0^{\infty}\frac{\mathrm{d}y}{1+y^{\alpha/2}x^{-\alpha/2}/\gamma_{th}}\bigg)$$
$$=\exp\bigg(-\eta_{D_m}\int_0^{x}\bigg(1-\frac{1}{1+y^{\alpha/2}x^{-\alpha/2}/\gamma_{th}}\bigg)\,\mathrm{d}y-\int_0^{\infty}\frac{\mathrm{d}y}{1+y^{\alpha/2}x^{-\alpha/2}/\gamma_{th}}\bigg)$$
$$=\exp\bigg(-\eta_{D_m}x-\eta_{D_m}\int_x^{\infty}\frac{\mathrm{d}y}{1+y^{\alpha/2}x^{-\alpha/2}/\gamma_{th}}-\int_0^{\infty}\frac{(1-\eta_{D_m})\,\mathrm{d}y}{1+y^{\alpha/2}x^{-\alpha/2}/\gamma_{th}}\bigg).$$

By taking $x=\pi\lambda_D z^2$ in the above series of equations, we get

$$\Delta_{D_m}\bigg(\frac{\pi\lambda_D z^2}{\beta_D}\bigg)$$
$$\xrightarrow[\beta_D\to 0]{}\exp\bigg(-\pi\eta_{D_m}\lambda_D z^2-\eta_{D_m}\int_{\pi\lambda_D z^2}^{\infty}\frac{\mathrm{d}y}{1+y^{\alpha/2}(\pi\lambda_D z^2)^{-\alpha/2}/\gamma_{th}}-\int_0^{\infty}\frac{(1-\eta_{D_m})\,\mathrm{d}y}{1+y^{\alpha/2}(\pi\lambda_D z^2)^{-\alpha/2}/\gamma_{th}}\bigg)$$
$$=\exp\bigg(-\pi\eta_{D_m}\lambda_D z^2-2\pi\lambda_D\eta_{D_m}\int_z^{\infty}\frac{v\;\mathrm{d}v}{1+v^{\alpha}z^{-\alpha}/\gamma_{th}}-(1-\eta_{D_m})\gamma_{th}^{2/\alpha}\pi\lambda_D z^2\int_0^{\infty}\frac{\mathrm{d}u}{1+u^{\alpha/2}}\bigg)$$
$$=\exp\bigg(-\pi\eta_{D_m}\lambda_D z^2-2\pi\lambda_D\eta_{D_m}\int_z^{\infty}\frac{v\;\mathrm{d}v}{1+v^{\alpha}/(\gamma_{th}z^{\alpha})}-\frac{2\pi^2(1-\eta_{D_m})(\gamma_{th}z^{\alpha})^{2/\alpha}\lambda_D}{\alpha\sin(2\pi/\alpha)}\bigg)$$
$$=\exp(-\pi\eta_{D_m}\lambda_D z^2)\mathcal{L}_{I_{D_m}}\bigg(\frac{\gamma_{th}z^{\alpha}}{P_D},z\bigg).\quad(73)$$

By the bounds given in (68) and (72) and the almost sure convergence proved in (69) and (73), one may apply the dominated convergence theorem to prove the convergence of (31) to (35) as β_D goes to zero.

Lastly, when the locations of the F-APs are modeled by a PPP, $\mathcal{L}_{I_F}$ is given by (27), and this concludes the proof.

APPENDIX C
PROOF OF THEOREM 5

We define the sequence $\{\epsilon_{F,i}\}_{i\in\mathbb{N}}$ analogously to $\{\epsilon_{D,i}\}_{i\in\mathbb{N}}$ in Appendix A. Additionally, for any $i \in \mathbb{N}$ we set

$$K_i := \bigcap_{k\in\mathbb{N}\setminus\{i\}} \big\{B_{F,k} \geq B_{F,i} \text{ or } \epsilon_{F,k} = 0 \text{ or } \Xi_{F,k} = 0\big\},$$

as well as

$$L_i := K_i \cap \{\epsilon_{F,i} = 1\} \cap \{\Xi_{F,i} = 1\}.$$

Letting $I_D = P_D h_q B_{D,q}^{-\alpha/2} + \sum_{l\neq q} P_D h_l B_{D,l}^{-\alpha/2}\Xi_{D,l}$ and proceeding as in (61), we have

$$\begin{aligned}
\tilde{\mathcal{P}}_{F_m} &= \mathbb{P}\left(\gamma_{F_m} \geq \gamma_{th},\ \|\mathbf{x}_{F_{m,o}}\| \leq r_F,\ \|\mathbf{x}_{D_{m,o}}\| > r_D\right) \\
&= \sum_{i=1}^{\infty}\sum_{q=1}^{\infty}\mathbb{P}\Bigg(\frac{P_F g_i B_{F,i}^{-\alpha/2}}{I_D + \sum_{k\in\mathbb{N}\setminus\{i\}} P_F g_k B_{F,k}^{-\alpha/2}\Xi_{F,k}} \geq \gamma_{th},\ B_{F,i} \leq r_F^2,\ B_{D,q} > r_D^2, \\
&\qquad\qquad \epsilon_{D,q} = 1,\ \Xi_{D,q} = 1,\ I_q,\ \epsilon_{F,i} = 1,\ \Xi_{F,i} = 1,\ K_i\Bigg) \\
&= \eta_{F_m}\beta_F\eta_{D_m}\beta_D \sum_{i=1}^{\infty}\sum_{q=1}^{\infty} T_{i,q}.
\end{aligned} \tag{74}$$

Additionally, $T_{i,q}$ above can be computed as

$$\begin{aligned}
T_{i,q} &\triangleq \mathbb{P}\left(g_i \geq \frac{\gamma_{th}B_{F,i}^{\alpha/2}}{P_F}\left(\sum_{k\in\mathbb{N}\setminus\{i\}} P_F g_k B_{F,k}^{-\alpha/2}\Xi_{F,k} + I_D\right),\ B_{F,i} \leq r_F^2,\ K_i,\ B_{D,q} > r_D^2,\ I_q\right) \\
&= \mathbb{E}\left[\exp\left(-\frac{\gamma_{th}B_{F,i}^{\alpha/2}}{P_F}\left(\sum_{k\in\mathbb{N}\setminus\{i\}} P_F g_k B_{F,k}^{-\alpha/2}\Xi_{F,k} + I_D\right)\right)\mathbb{1}_{\left\{B_{F,i}\leq r_F^2,\ K_i\right\}}\mathbb{1}_{\left\{B_{D,q}>r_D^2,\ I_q\right\}}\right] \\
&= \mathbb{E}\Bigg[\prod_{k\in\mathbb{N}\setminus\{i\}}\exp\left(-\gamma_{th}B_{F,i}^{\alpha/2}g_k B_{F,k}^{-\alpha/2}\Xi_{F,k}\right)\mathbb{1}_{\left\{B_{F,i}\leq r_F^2,\ K_i\right\}}\exp\left(-\frac{\gamma_{th}B_{F,i}^{\alpha/2}}{P_F}P_D h_q B_{D,q}^{-\alpha/2}\right) \\
&\qquad\times\prod_{l\in\mathbb{N}\setminus\{q\}}\exp\left(-\frac{\gamma_{th}B_{F,i}^{\alpha/2}}{P_F}P_D h_l B_{D,l}^{-\alpha/2}\right)\mathbb{1}_{\left\{B_{D,q}>r_D^2,\ I_q\right\}}\Bigg] \\
&= \mathbb{E}\Bigg[\prod_{k\in\mathbb{N}\setminus\{i\}}\frac{\mathbb{1}_{\left\{B_{F,i}\leq r_F^2,\ K_i\right\}}}{1+\gamma_{th}B_{F,i}^{\alpha/2}B_{F,k}^{-\alpha/2}\Xi_{F,k}}\cdot\frac{1}{1+\frac{\gamma_{th}B_{F,i}^{\alpha/2}}{P_F}P_D B_{D,q}^{-\alpha/2}}\prod_{l\in\mathbb{N}\setminus\{q\}}\frac{\mathbb{1}_{\left\{B_{D,q}>r_D^2,\ I_q\right\}}}{1+\frac{\gamma_{th}B_{F,i}^{\alpha/2}}{P_F}P_D B_{D,l}^{-\alpha/2}}\Bigg]
\end{aligned}$$

$$= \mathbb{E}\left[\prod_{k\in\mathbb{N}\setminus\{i\}} \frac{\mathbb{1}_{\left\{B_{F,i}\leq r_F^2,\ K_i\right\}}}{1+\gamma_{th}B_{F,i}^{\alpha/2}B_{F,k}^{-\alpha/2}\Xi_{F,k}} T_q\left(\frac{\gamma_{th}B_{F,i}^{\alpha/2}}{P_F}\right)\right], \tag{75}$$

where, recalling that $A_{\eta_{D_m},\beta_D,l}$ is defined in (34), we set

$$\begin{aligned}
T_q(\tau) &\triangleq \mathbb{E}\left[\frac{1}{1+\tau P_D B_{D,q}^{-\alpha/2}}\prod_{l\in\mathbb{N}\setminus\{q\}}\frac{\mathbb{1}_{\left\{B_{D,q}>r_D^2,\ I_q\right\}}}{1+\tau P_D B_{D,l}^{-\alpha/2}}\right]\\
&= \mathbb{E}\left[\frac{1}{1+\tau P_D B_{D,q}^{-\alpha/2}}\prod_{l\in\mathbb{N}\setminus\{q\}}\left(1-\beta_D+\frac{\beta_D}{1+\tau P_D B_{D,l}^{-\alpha/2}}\mathbb{1}_{\left\{B_{D,l}\geq B_{D,q}\text{ or }\epsilon_{D,l}=0\right\}}\right)\mathbb{1}_{\left\{B_{D,q}>r_D^2\right\}}\right]\\
&= \mathbb{E}\left[\frac{1}{1+\tau P_D B_{D,q}^{-\alpha/2}}\prod_{l\in\mathbb{N}\setminus\{q\}}\left(1-\beta_D+\frac{\eta_{D_m}\beta_D\mathbb{1}_{\left\{B_{D,l}>B_{D,q}\right\}}}{1+\tau P_D B_{D,l}^{-\alpha/2}}+\frac{(1-\eta_{D_m})\beta_D}{1+\tau P_D B_{D,l}^{-\alpha/2}}\right)\mathbb{1}_{\left\{B_{D,q}>r_D^2\right\}}\right]\\
&= \int_{r_D^2}^{\infty}\frac{1}{1+\tau P_D y^{-\alpha/2}}f_{B_{D,q}}(y)\prod_{l\in\mathbb{N}\setminus\{q\}}A_{\eta_{D_m},\beta_D,l}\left(\frac{\pi\lambda_D y}{\beta_D},\tau P_D\left(\frac{\pi\lambda_D}{\beta_D}\right)^{\alpha/2}\right)\mathrm{d}y.
\end{aligned} \tag{76}$$

Here, we have skipped some steps since the arguments are identical to those in (62). Defining $\hat{\mathcal{L}}_{I_D}(\tau)=\eta_{D_m}\beta_D\sum_{q=1}^{\infty}T_q(\tau)$, by the change of variables $z=\sqrt{y}$, we find that $\hat{\mathcal{L}}_{I_D}(\tau)$ is equal to (52).

Then, by plugging (75) into (74) and again proceeding as in Appendix A, we rewrite $\tilde{\mathcal{P}}_{F_m}$ as

$$\begin{aligned}
\tilde{\mathcal{P}}_{F_m} &= \eta_{F_m}\beta_F\eta_{D_m}\beta_D\sum_{i=1}^{\infty}\sum_{q=1}^{\infty}\mathbb{E}\left[T_q\left(\frac{\gamma_{th}B_{F,i}^{\alpha/2}}{P_F}\right)\prod_{k\in\mathbb{N}\setminus\{i\}}\frac{\mathbb{1}_{\left\{B_{F,i}\leq r_F^2,\ K_i\right\}}}{1+\gamma_{th}B_{F,i}^{\alpha/2}B_{F,k}^{-\alpha/2}\Xi_{F,k}}\right]\\
&= \eta_{F_m}\beta_F\sum_{i=1}^{\infty}\mathbb{E}\left[\hat{\mathcal{L}}_{I_D}\left(\frac{\gamma_{th}B_{F,i}^{\alpha/2}}{P_F}\right)\prod_{k\in\mathbb{N}\setminus\{i\}}\frac{\mathbb{1}_{\left\{B_{F,i}\leq r_F^2,\ K_i\right\}}}{1+\gamma_{th}B_{F,i}^{\alpha/2}B_{F,k}^{-\alpha/2}\Xi_{F,k}}\right]\\
&= \eta_{F_m}\beta_F\int_0^{\frac{\pi\lambda_F}{\beta_F}r_F^2}\hat{\mathcal{L}}_{I_D}\left(\frac{\gamma_{th}}{P_F}\left(\frac{\beta_F u}{\pi\lambda_F}\right)^{\alpha/2}\right)\exp(-u)\,\Upsilon_{F_m}(u)\Delta_{F_m}(u)\,\mathrm{d}u,
\end{aligned} \tag{77}$$

where $\Upsilon_{F_m}(z)$ and $\Delta_{F_m}(z)$ are defined in (38) and (39), respectively. Finally, by the change of variable $z=\sqrt{\beta_F u/(\pi\lambda_F)}$, we obtain (51).

It remains to prove that $\hat{\mathcal{L}}_{I_D}$ is given by (55) when $\Phi_D\sim PPP(\lambda_D)$, and we prove this by taking the limit as β_D goes to zero. For this, it suffices to note that the proof of Appendix B can be adapted to our setting by replacing γ_{th} with $\tau P_D z^{-\alpha}$; indeed this is clear by comparing the definitions (32)-(33) with those in (53)-(54). In particular, for any fixed $z>0$, by (69) we deduce

$$\exp\left(-\frac{\pi\lambda_D z^2}{\beta_D}\right)\hat{\Upsilon}_{D_m}\left(\frac{\pi\lambda_D z^2}{\beta_D},z^2,\tau\right)\xrightarrow[\beta_D\to 0]{}1,$$

and by (73) we get

$$\hat{\Delta}_{D_m}\left(\frac{\pi\lambda_D z^2}{\beta_D}, z^2, \tau\right) \xrightarrow[\beta_D\to 0]{}$$
$$\exp\left(-\eta_{D_m}\pi\lambda_D z^2 - \eta_{D_m}\int_{\pi\lambda_D z^2}^{\infty}\frac{\mathrm{d}y}{1+y^{\alpha/2}(\pi\lambda_D)^{-\alpha/2}/(\tau P_D)} - \int_0^{\infty}\frac{(1-\eta_{D_m})\,\mathrm{d}y}{1+y^{\alpha/2}(\pi\lambda_D)^{-\alpha/2}/(\tau P_D)}\right)$$
$$= \exp(-\pi\eta_{D_m}\lambda_D z^2)\mathcal{L}_{I_{D_m}}(\tau, z).$$

The dominated convergence theorem along with the almost everywhere convergence yields (55).

REFERENCES

[1] J. G. Andrews, S. Buzzi, W. Choi, S. V. Hanly, A. Lozano, A. C. K. Soong, and J. C. Zhang, "What will 5G be?," *IEEE J. Sel. Areas Commun.*, vol. 32, pp. 1065–1082, Jun. 2014.

[2] M. Peng, S. Yan, K. Zhang, and C. Wang, "Fog-computing-based radio access networks: Issues and challenges," *IEEE Netw.*, vol. 30, pp. 46–53, Jul. 2016.

[3] M. Peng, Y. Sun, X. Li, Z. Mao, and C. Wang, "Recent advances in cloud radio access networks: System architectures, key techniques, and open issues," *IEEE Commun. Surveys Tuts.*, vol. 18, pp. 2282–2308, Third Quart. 2016.

[4] S.-H. Park, O. Simeone, O. Sahin, and S. Shamai, "Robust and efficient distributed compression for cloud radio access networks," *IEEE Trans. Veh. Technol.*, vol. 62, pp. 692–703, Feb. 2013.

[5] J. Kang, O. Simeone, J. Kang, and S. Shamai, "Layered downlink precoding for C-RAN systems with full dimensional MIMO," *IEEE Trans. Veh. Technol.*, vol. 66, pp. 2170–2182, Mar. 2017.

[6] S. A. R. Zaidi, A. Imran, D. C. McLernon, and M. Ghogho, "Characterizing coverage and downlink throughput of cloud empowered HetNets," *IEEE Commun. Lett.*, vol. 19, pp. 1013–1016, Jun. 2015.

[7] F. A. Khan, H. He, J. Xue, and T. Ratnarajah, "Performance analysis of cloud radio access networks with distributed multiple antenna remote radio heads," *IEEE Trans. Signal process.*, vol. 63, pp. 4784–4799, Sep. 2015.

[8] M. Peng, S. Yan, and H. V. Poor, "Ergodic capacity analysis of remote radio head associations in cloud radio access networks," *IEEE Wireless Commun. Lett.*, vol. 3, pp. 365–368, Aug. 2014.

[9] J. Park and R. W. Heath, "Low complexity antenna selection for low target rate users in dense cloud radio access networks," *IEEE Trans. Wireless Commun.*, vol. 15, pp. 6022–6032, Sep. 2016.

[10] Cisco, "Cisco visual networking index: Global mobile data traffic forecast update, 2016-2021," 2017.

[11] X. Wang, M. Chen, T. Taleb, A. Ksentini, and V. C. M. Leung, "Cache in the air: exploiting content caching and delivery techniques for 5G systems," *IEEE Commun. Mag.*, vol. 52, pp. 131–139, Feb. 2014.

[12] K. Shanmugam, N. Golrezaei, A. G. Dimakis, A. F. Molisch, and G. Caire, "Femtocaching: Wireless content delivery through distributed caching helpers," *IEEE Trans. Inf. Theory*, vol. 59, pp. 8402–8413, Dec. 2013.

[13] M. Ji, G. Caire, and A. F. Molisch, "Fundamental limits of caching in wireless D2D networks," *IEEE Trans. Inf. Theory*, vol. 62, pp. 849–869, Feb. 2016.

[14] S. Tamoor-ul-Hassan, M. Bennis, P. H. J. Nardelli, and M. Latva-aho, "Caching in wireless small cell networks: A storage-bandwidth tradeoff," *IEEE Commun. Lett.*, vol. 20, pp. 1175–1178, Jun. 2016.

[15] E. Baştuğ, M. Bennis, M. Kountouris, and M. Debbah, "Cache-enabled small cell networks: modeling and tradeoffs," *EURASIP J. Wireless Commun. Netw.*, vol. 41, pp. 1–11, Dec. 2015.

[16] D. Malak, M. Al-Shalash, and J. G. Andrews, "Optimizing content caching to maximize the density of successful receptions in device-to-device networking," *IEEE Trans. Commun.*, vol. 64, pp. 4365–4380, Oct. 2016.

[17] M. Afshang, H. S. Dhillon, and P. H. J. Chong, "Fundamentals of cluster-centric content placement in cache-enabled device-to-device networks," *IEEE Trans. Commun.*, vol. 64, pp. 2511–2526, Jun. 2016.

[18] S.-H. Park, O. Simeone, and S. Shamai, "Joint optimization of cloud and edge processing for fog radio access networks," *IEEE Trans. Wireless Commun.*, vol. 15, pp. 7621–7632, Nov. 2016.

[19] A. Sengupta, R. Tandon, and O. Simeone, "Fog-aided wireless networks for content delivery: Fundamental latency tradeoffs," [Online] Available: https://arxiv.org/pdf/1605.01690.pdf.

[20] Z. Zhao, M. Peng, Z. Ding, W. Wang, and H. V. Poor, "Cluster content caching: An energy-efficient approach to improve quality of service in cloud radio access networks," *IEEE J. Sel. Areas Commun.*, vol. 34, pp. 1207–1221, May 2016.

[21] S. Yan, M. Peng, and W. Wang, "User access mode selection in fog computing based radio access networks," in *Proc. IEEE Int. Conf. Commun. (ICC)*, May 2016, pp. 1-6.

[22] A. Guo and M. Haenggi, "Spatial stochastic models and metrics for the structure of base stations in cellular networks," *IEEE Trans. Wireless Commun.*, vol. 12, pp. 5800–5812, Nov. 2013.

[23] S.-R. Cho and W. Choi, "Energy-efficient repulsive cell activation for heterogeneous cellular networks," *IEEE J. Sel. Areas Commun.*, vol. 31, pp. 870–882, May 2013.

[24] Y. Li, F. Baccelli, H. S. Dhillon, and J. G. Andrews, "Statistical modeling and probabilistic analysis of cellular networks with determinantal point processes," *IEEE Trans. Commun.*, vol. 63, pp. 3405–3422, Sep. 2015.

[25] H.-B. Kong, P. Wang, D. Niyato, and Y. Cheng, "Modeling and analysis of wireless sensor networks with/without energy harvesting using Ginibre point processes," *IEEE Trans. Wireless Commun.*, vol. 16, pp. 3700–3713, Jun. 2017.

[26] H. B. Kong, I. Flint, P. Wang, D. Niyato, and N. Privault, "Exact performance analysis of ambient RF energy harvesting wireless sensor networks with Ginibre point process," *IEEE J. Sel. Areas Commun.*, vol. 34, pp. 3769–3784, Dec. 2016.

[27] N. Deng, W. Zhou, and M. Haenggi, "The Ginibre point process as a model for wireless networks with repulsion," *IEEE Trans. Wireless Commun.*, vol. 14, pp. 107–121, Jan. 2015.

[28] I. Nakata and N. Miyoshi, "Spatial stochastic models for analysis of heterogeneous cellular networks with repulsively deployed base stations," *Performance Evaluation*, vol. 78, pp. 7–17, Aug. 2014.

[29] J. S. Gomez, A. Vasseur, A. Vergne, P. Martins, L. Decreusefond, and W. Chen, "A case study on regularity in cellular network deployment," *IEEE Wireless Commun. Lett.*, vol. 4, pp. 421–424, Aug. 2015.

[30] L. Decreusefond, I. Flint, and A. Vergne, "Efficient simulation of the Ginibre point process," *Adv. Appl. Probab.*, vol. 52, pp. 1–21, Oct. 2015.

[31] T. Shirai and Y. Takahashi, "Random point fields associated with certain Fredholm determinants I: Fermion, Poisson and boson point processes," *J. Functional Anal.*, vol. 205, pp. 414–463, Apr. 2003.

[32] A. Goldman, "The Palm measure and the Voronoi tessellation for the Ginibre process," *Ann. Appl. Probab.*, vol. 20, pp. 90–128, 2010.

[33] M. Zink, K. Suh, Y. Gu, and J. Kurose, "Characteristics of youtube network traffic at a campus network-measurements, models, and implications," *Comput. Netw.*, vol. 53, pp. 501–514, Mar. 2009.

[34] M. Haenggi, *Stochastic geometry for wireless networks*. Cambridge, U.K.: Cambridge Univ. Press, 2012.

[35] A. M. Cohen, *Numerical methods for Laplace transform inversion*. New York, NY, USA: Springer, 2007.

[36] K. J. Hollenbeck, *invlap.m: A Matlab function for numerical inversion of Laplace transforms by the de Hoog algorithm*. https://www.isva.dtu.dk/staff/karl/invlap.htm, 1998.

[37] A. H. Sakr and E. Hossain, "Cognitive and energy harvesting-based D2D communication in cellular networks: Stochastic geometry modeling and analysis," *IEEE Trans. Commun.*, vol. 63, pp. 1867–1880, May 2015.